


RESEARCH

Open Access



# Loading tea polyphenols enhances the repair of human umbilical cord mesenchymal stem cell sheet after spinal cord injury

Yulin Zhao<sup>1,2†</sup>, Cong Ye<sup>1,2†</sup>, Heng Wang<sup>1†</sup>, Cheng Chen<sup>1</sup>, Yang Lu<sup>1</sup>, Changwei Yang<sup>1</sup>, Tao Xu<sup>2</sup>, Yuchen Zhou<sup>1,2</sup>, Zhengchao Wu<sup>1,2</sup>, Xianrui Song<sup>1,2</sup>, Zhenyang Zhu<sup>2</sup>, Zongze Yang<sup>1,2</sup> and Xiaoqing Chen<sup>1\*</sup> 

## Abstract

**Background** Spinal cord injury (SCI) is a devastating central nervous system disorder that remains a global health challenge. SCI-induced oxidative stress in the postinjury microenvironment limits tissue repair by provoking the excessive production of reactive oxygen species (ROS). Tea polyphenols (TP), as a natural plant polyphenol, could effectively reduce ROS. In recent years, stem cell-based therapy combined with cell sheet technology has been widely used in the treatment of SCI. Therefore, we constructed human umbilical cord mesenchymal stem cell sheet loaded with TP (CS-TP) and evaluated their therapeutic effects and mechanisms both in vitro and in vivo in SCI rats.

**Methods** Human umbilical cord mesenchymal stem cell sheet (CS) were prepared by temperature-responsive cell culture method and successfully loaded with TP. The protective effect of CS and CS-TP on cells against oxidative stress was tested by Live/Dead cell staining and CCK-8 assay. CS and CS-TP were co-cultured with PC12 cells and human umbilical vein endothelial cells (HUVECs), respectively, and their effects on reducing ROS production were evaluated using flow cytometry and ROS fluorescence assays. Immune fluorescence (IF) and Western blot analysis of the mechanism by which CS-TP affects PC12 cells and HUVECs in vitro. Wound healing assay, transwell Chamber invasion experiment and tube formation assay were performed to evaluate the effects of CS and CS-TP on the biological behaviors of HUVECs. (Basso-Beattie-Bresnahan) BBB scores and gait analysis were performed to assess the recovery of motor function in rats. Molecular modeling is used to study the affinity between the main active ingredient epigallocatechin gallate (EGCG) in TP and target proteins. Western blot analyzes the mechanism of action of CS and CS-TP in SCI animals and the expression levels of antioxidant proteins. Tissue IF staining was used to evaluate angiogenesis, neuron regeneration and axonal extension.

**Results** Compared with CS, CS-TP could effectively reduce cellular ROS production and increase cell viability under high oxidative stress conditions and significantly enhance its biological activity. In vitro, CS-TP can significantly activate the Keap-1/Nrf2/HO-1 pathway, thereby affecting PC12 cells and HUVECs. After transplantation in SCI rats, CS-TP also activates the Keap-1/Nrf2/HO-1 pathway, influencing the repair of SCI and upregulating the expression

<sup>†</sup>Yulin Zhao, Cong Ye, and Heng Wang have contributed equally to this study.

\*Correspondence:

Xiaoqing Chen

chenxiaoqing@ntu.edu.cn

Full list of author information is available at the end of the article



© The Author(s) 2025. **Open Access** This article is licensed under a Creative Commons Attribution-NonCommercial-NoDerivatives 4.0 International License, which permits any non-commercial use, sharing, distribution and reproduction in any medium or format, as long as you give appropriate credit to the original author(s) and the source, provide a link to the Creative Commons licence, and indicate if you modified the licensed material. You do not have permission under this licence to share adapted material derived from this article or parts of it. The images or other third party material in this article are included in the article's Creative Commons licence, unless indicated otherwise in a credit line to the material. If material is not included in the article's Creative Commons licence and your intended use is not permitted by statutory regulation or exceeds the permitted use, you will need to obtain permission directly from the copyright holder. To view a copy of this licence, visit <http://creativecommons.org/licenses/by-nc-nd/4.0/>.

of SOD1 and SOD2. CS-TP can more effectively promote angiogenesis, neuronal regeneration, and axonal extension in injured spinal cords, greatly improving the motor function of the rats.

**Conclusion** CS-TP not only significantly enhances the resistance of CS to ROS, activates the Keap-1/Nrf2/HO-1 pathway, and regulates the level of antioxidant proteins in the body. Compared to CS, it can also more effectively increase the number of new blood vessels, promote neuron regeneration and axon extension, thereby more effectively repairing SCI.

**Keywords** Cell sheet, Human umbilical cord mesenchymal cells, Angiogenesis, Tea polyphenols, Spinal cord injury

## Introduction

Spinal cord injury (SCI) represents temporary or permanent irreversible damage to sensory and motor functions due to injury of the spinal cord tissue [1]. SCI is categorized into two phases, termed primary and secondary injury [2, 3]. Primary injury refers to the initial impact inducing spinal cord damage, during which neural network and the blood barrier are disrupted leading to compromised blood supply. Secondary injury encompasses a cascade of severe consequences occurring after the primary injury, such as extensive neuronal death, massive inflammatory response, and scar formation. Due to sustained ischemia, inflammation, edema, and other secondary injury insults, excessive ROS and free radicals are generated and released [4, 5], and these strong oxidants accumulate in the tissue, leading to cellular dysfunctions of neurons and microvascular genesis, further resulting in neurological deficits [6–8].

Improving blood supply to the SCI is considered a major strategy for early intervention since ischemia creates an unfavorable microenvironment in the injury site. Post-traumatic angiogenesis ensures nutritional support, which plays a positive role in establishing and maintaining the homeostasis of neural networks [9–11]. Axonal regeneration has also been shown to grow along blood vessels [12–14]. However, high levels of oxidative stress and a poor microenvironment restrict endogenous repair of microvasculature and regeneration of axons after SCI [15, 16]. Therefore, rapidly balancing the oxidative stress environment in the spinal cord is an important pathway to guarantee angiogenesis, restore blood supply, and protect spinal cord vessels.

MSCs (mesenchymal stem cells)-based facilitation of angiogenesis holds great promise in SCI. Recent investigations have demonstrated that the major pathway by which MSCs promote SCI angiogenesis is dependent on their paracrine mechanism. MSCs can promote the restoration of blood supply to the injury area through paracrine production of beneficial cytokines, EVs, and so on [17–19]. The majority of researchers use intrathecal injections and intravenous injections to transplant MSCs. These methods have proven effective [20, 21]. The advent of engineered scaffolds using cellular sheet technology

provides novel avenues for cell delivery [22]. The cell sheet is mainly composed of cells and the extracellular matrix secreted by the cells themselves. The ECM not only provides a natural growth site for cells but also acts as a bioactive scaffold that bridges the transected ends of the injury site. There have been many studies on the treatment of SCI using cell sheet technology [23, 24].

In the biomedical area, TP, as a class of cross-linking polyphenols, widely existed in many plants, possessing antioxidants, anti-inflammatory, and antibacterial properties along with excellent biocompatibility [24, 25]. However, an important issue for systematic applications of TP is that it is still challenging for TP to exert their valid therapeutic effects locally, and these limitations hamper the clinical developments of TP as potential therapeutic agents. In addition, polyphenols like TP have the ability to adhere by hydrogen-bonding collagen [26–29]. To be specific, the catechol structure in TP is easily oxidized under alkaline condition to the form of quinones, which can subsequently undergo Michael addition or Schiff base reaction with amino groups, thus providing a stable linkage with amino or thiol groups. It is noteworthy that the CS containing ECM is rich in collagen and fibrin, which provides the possibility for loading TP onto the CS.

Inspired by the concepts, we cross-linked CS with TP to fabricate the CS-TP to facilitate SCI repair. Although cell sheet has been used to improve neural recovery after SCI in previous studies, there are few studies on the modification of cell sheet and the effects of cell sheet on HUVECs or vascular system of spinal cord under oxidative stress conditions. In this study, we demonstrated the potentials of CS-TP in SCI treatment and evaluated its safety and efficacy, aiming to explore more effective approaches of cell sheet-based therapy of SCI.

## Materials and methods

### Animals

Female Sprague-Dawley (SD) rats, aged 8 weeks and weighing approximately 220 g, were selected from Nantong University Laboratory Animal Center for the experiment. The animals had free access to standard rodent food and water, and were kept in a stable and controlled

environment (50% humidity, 22–26 °C, 12-h light–dark cycle).

#### Isolation, culture, and identification of hUC-MSCs

Human umbilical cord mesenchymal cells (hUC-MSCs) were isolated from umbilical cord collected after cesarean section. Specifically, Wharton's jelly tissues were isolated from umbilical cords, cut into pieces, and cultured in DMEM/F12 (Gibco) supplemented with 10% FBS (Procell) and 1% penicillin–streptomycin in a humidified atmosphere with 5% CO<sub>2</sub> at 37 °C. When the cells reached 70% to 80% confluence, they were digested with 0.25% trypsin–EDTA (NCM Biotech) and passaged at a ratio of 1:2. To characterize the multipotent differentiation capability of hUC-MSCs, adipogenic, osteogenic, and chondrogenic differentiation assays were performed. Flow cytometry (BD Biosciences, FACSCalibur™) was used to characterize the hUC-MSCs after incubation with antibodies targeting specific surface antigens, such as CD29, CD44, CD73, CD90, CD105, CD45, and HLA-DR. BD FACS Aria II flow cytometer (BD Biosciences) was used for final quantitative analysis. Flow Cytometry data analysis software (FlowJo V10.8.1, FlowJo, LLC) was used for data analysis.

#### Fabrication and characterization of CS and CS-TP

To prepare CS, the hUC-MSCs expanded to the fifth passage (P5) were suspended and seeded onto the surface of 3.5 cm thermo responsive cell culture dishes (Thermo) at a density of  $1.3 \times 10^5$  cells/cm<sup>2</sup>. When the cell confluence reached 90–100%, vitamin C (50 µg/mL) was added into the culture medium to facilitate the generation of ECM. The medium was changed every 2 days and incubated at 37 °C with 5% CO<sub>2</sub> for 2 weeks, after which the incubation temperature was reduced to 20 °C for 40 min. The hUC-MSCs will spontaneously form CS, which are obtained after the transfer membrane. The morphology of CS was observed using an optical microscope and a scanning electron microscope (SEM). Finally, H&E staining, collagen-1 (Proteintech), and IF staining of 4',6-diamidino-2-phenylindole (DAPI) were performed on the cryosections of the CS. In the preparation of CS-TPs, all the other steps remained the same, except that TP with a concentration of 5 µM was added to the medium that was replaced. The specific preparation method for the TP conditional culture medium is as follows: dissolve 115 µg of TP powder in 50 ml of complete culture medium and replace the medium with 2 ml each time. TP (Tea polyphenol, purity 99%, CAS No.: 84650–60-2), purchased from Shanghai Macklin Biochemical Co., Ltd.

#### Protective effects on cells in vitro

Using a live/dead cell staining kit (Sigma) to evaluate the protective effect of CS and CS-TP on cells, where live cells are stained green by calcein-AM and dead cells are stained red by propidium iodide. Fluorescent images are observed using a microscope (Leica). PC12 cells and HUVECs were stimulated overnight with a basal medium containing H<sub>2</sub>O<sub>2</sub>. Subsequently, CS and CS-TP were co-cultured with PC12 cells and HUVECs. Among them, the Control group was the normal cell group, the H<sub>2</sub>O<sub>2</sub> group was not treated after H<sub>2</sub>O<sub>2</sub> stimulation, and the CS group and CS-TP group were the treatment groups with CS and CS-TP added. All the following vitro experiments use this grouping. After 72 h, the cells were stained using a live-dead staining kit. Additionally, the cell viability of PC12 cells and HUVECs at different time points was measured using a CCK-8 detection kit.

#### ROS generation detection

Using a ROS assay kit (Beyotime), the intracellular ROS levels were measured, with fluorescence intensity being proportional to the ROS levels. In simple terms, PC12 cells and HUVECs were first seeded in 6-well plates and, once they reached 70–80% confluence, were incubated overnight in medium containing 500 µM. They were then cultured for 24 h according to different treatment groups. DCFH-DA was added and incubated in the dark at 37 °C for 30 min, then fixed with 4% PFA for 20 min. Fluorescence was measured using a fluorescence microscope (Zeiss). Following the same steps as above, after removing CS and CS-TP, the cells were centrifuged, and the supernatant was removed. DCFH-DA reagent was added, and after washing, the cells were analyzed using flow cytometry.

#### Cell wound healing (cell migration) assay

A two-dimensional wound scratch assay was conducted on a 6-well plate to assess the migration of HUVECs. HUVECs were seeded in a 6-well plate ( $5 \times 10^5$  cells per well) and treated overnight in serum-free medium containing 500 µM H<sub>2</sub>O<sub>2</sub>. A scratch was made on the adherent cells at the radial center of each well using a 200 µl sterile pipette tip, followed by three washes with PBS to remove floating cells, and the scratch was immediately observed under a microscope. HUVECs were treated with different treatment groups. To detect the rate of cell migration and exclude components related to cell proliferation, HUVECs were co-incubated with the anti-mitotic agent mitomycin (Sigma). After 12 h, the wound was observed using an inverted phase-contrast microscope. The experiment was repeated three times, and the un migrated cell area was determined using

ImageJ v1.4 (National Institutes of Health, Bethesda, MD, USA). The healing index was analyzed as follows:  $\text{Healing Index} = (\text{Initial Area} - \text{Remaining Area}) / \text{Initial Area} \times 100\%$ .

#### Transwell chamber invasion experiment

Conduct the experiment using a Transwell migration chamber. On ice, dilute Matrigel matrix glue with DMEM/F12 medium at a ratio of 1:8. Place the Transwell chamber into a 24-well plate, adding 100  $\mu\text{L}$  of the diluted Matrigel matrix gel (Corning) to each chamber. Incubate at 37 °C for 1 h to allow the gel to fully solidify. Seed HUVECs at a density of  $5 \times 10^4$  cells/well in the upper chamber of the Transwell. Add 600  $\mu\text{L}$  of complete culture medium and CS, CS-TP respectively to the lower chamber. After 18 h, remove the non-migrated cells on the surface of the upper chamber of the Transwell using a sterile cotton swab. Rinse 3 times with PBS, fix with 4% paraformaldehyde for half an hour, and rinse 3 times with PBS again. Add 500  $\mu\text{L}$  of crystal violet solution (Byotime) to the lower chamber of the Transwell and stain for half an hour, followed by 3 washes with PBS. After drying, place a blank slide on the microscope stage and invert the upper chamber of the Transwell onto the slide for photographing.

#### Tube formation assay

Place CS and CS-TP at the bottom of a 24-well plate. Pre-dilute Matrigel matrix gel and DMRM/F12 basal medium in a 1:1 ratio on ice. Add 200  $\mu\text{L}$  of the matrix gel dilution to each well of the 24-well plate and leave it in a 37 °C incubator for 1 h to allow the matrix gel to solidify completely. Seed  $\text{H}_2\text{O}_2$ -treated HUVECs onto the matrix gel and incubate in a 37 °C cell incubator for 6 h. Observe the tube formation under an inverted microscope. Use ImageJ software (NIH, Bethesda, USA) to quantify the number of nodes/ meshes /branches/ junctions of capillaries and tubular structures.

#### Establishment of SCI model and implantation of CS and CS-TP

CS and CS-TP were harvested on the day of surgery and maintained in standard culture medium until transplantation. Female SD rats were anesthetized under pentobarbital (1.2 g/kg, i.p.). We performed a laminectomy at T10 and then transected the spinal cord from the center to the left side using a specially designed double-row scalpel (with approximately 2 mm intervals), creating a left-sided hemisection of the rat spinal cord. The rats were randomly divided into four groups: Rats were randomly divided into four groups ( $n=15/\text{group}$ ): (1) Control group; (2) SCI group (injury treatment only); (3) CS group (implantation of CS at the spinal cord defect site); (4)

CS-TP group (implantation of CS-TP at the spinal cord defect site). Each group consisted of 15 rats. The muscles, fascia, and epidermis were then carefully sutured, and the incision was disinfected with iodine. The rodents were subsequently injected with penicillin ( $40 \times 10^5$  units/rat/day, i.m.) and buprenorphine (0.01 mg/kg, i.m). The bladder was manually emptied three times a day until reflex bladder control was restored. The specific method for animal euthanasia is as follows: Place the mice in an individually ventilated cage (ivc), cover the cage lid, connect the  $\text{CO}_2$  pipeline, and open the gas valve, infusing  $\text{CO}_2$  into the chamber at a rate of 10% to 30% of the euthanasia box volume per minute. Once the mice pass out and lose motor ability, increase the  $\text{CO}_2$  flow rate, ensuring it does not exceed a maximum flow rate of 0.5 Kpa. After confirming the mice are immobile, not breathing, and pupils are dilated, turn off the  $\text{CO}_2$ , and observe for an additional 2 min to ensure death. The animal carcasses are sealed in white transparent self-sealing bags and sent to the Nantong University Laboratory Animal Center for centralized harmless disposal.

#### Functional recovery and footprint analysis

The BBB locomotor rating scale is used for evaluation at 0, 7, 14, 21, and 28 days. It employs a 0–21-point scale. The test is conducted at the same time on the same day for all groups, once a week within 4 weeks after SCI. This scoring system is based on observing hindlimb movement in an open field over a five-minute period. Three experimenters conducted a double-blind assessment to determine scores for joint movement, limb coordination, and trunk stability. Functional recovery of hindlimb function in rats was assessed using the CatWalk XT system (Noldus Information Technology, Wageningen, the Netherlands). Briefly, paw prints were collected 4 weeks after SCI and footprint intensity was measured. Parameters were calculated using the software. CatWalk stride length was determined as ratio of left hindlimb stride length to right hindlimb stride length. The print area was determined to quantify foot placement, and other parameters were calculated by dividing the left hindpaw area by the right hindpaw area. To account for confounding factors such as weight and paw size, the mean intensity was calculated by dividing the absolute value of the difference between right and left hindpaw intensity by the intensity of the right hindpaw.

#### Western blot

The expressions of Keap-1 (Proteintech), Nrf2 (Abcam), PCNA (Proteintech), HO-1 (Abcam), SOD-1 (Proteintech), SOD-2 (Proteintech), GAPDH (Proteintech) and  $\beta$ -actin (Abcam) were detected using Western blotting. Cell protein extraction requires lysing cells with RIPA



buffer. Tissue protein extraction requires homogenizing the tissue using a homogenizer, collecting the homogenate, and then centrifuging it at 15,000 rpm for 10 min at 4 °C. Protein concentration is then determined using a BCA protein assay kit. The supernatant in the tube was carefully aspirated and added to the loading buffer and boiled for 10 min, and the experimental protein sample was obtained and stored at – 20 °C. All operations were carried out according to the instructions of the kit. In addition, the proteins were separated using Sodium Dodecyl Sulfate Polyacrylamide Gel Electrophoresis (SDS-PAGE) and PVDF membrane. After blocking for 2 h, the blot was incubated with the primary antibody overnight. The blot was subsequently incubated with the secondary antibody. The determination steps for organ proteins are like those for cellular proteins. All original blot images were available in Appendix S1.

To analyze the effect of CS and CS-TP on Nrf2 translocation, cytoplasmic and nuclear components were isolated from different groups using a nuclear and cytoplasmic protein extraction kit (Bestbio Science). After washing with PBS, the cells were collected, and the supernatant was extracted using a cytoplasmic lysis buffer to obtain the cytoplasmic components. The precipitate was then added to the nuclear lysis buffer and centrifuged at 10,000 rpm to obtain the nuclear components. The expression of Nrf2 in the cytoplasm and nucleus was analyzed to assess Nrf2 translocation.

### Molecular modeling

The molecular weight and 2D and 3D structure of compounds were retrieved from PubChem database (<https://pubchem.ncbi.nlm.nih.gov/>) while the 3D conformation of proteins was obtained from the Protein Data Bank (<https://www.rcsb.org/>). To objectively illustrate whether the enhanced oxidative capacity of CS-TP and the activation of related pathways are derived from the loading of EGCG, we selected EGCG (molecular formula:  $C_{22}H_{18}O_{11}$ ; molecular weight: 458.372) for relevant simulation analysis with Nrf2 and HO-1. We selected compounds as ligands and identified proteins as their receptor counterparts. Parameters such as grid box center position and dimensions were set according to the interaction profile of the small molecules with their protein targets. Exhaustive batch docking was performed using AutoDock4, and the results were carefully analyzed. For better visualization of the binding interactions between compounds and their protein counterparts, PyMOL 2.1 software was used. Following docking, the lead compounds were visualized with PyMOL and the types of interactions such as hydrogen bonding,  $\pi$ – $\pi$  stacking, and hydrophobic interactions were analyzed.

### IF staining of cells and tissues

**Cell IF assay:** Cells are seeded on a 6-well plate and fixed with 4% paraformaldehyde at room temperature for 20 min, followed by three washes. The sections are then incubated with 0.3% Triton X-100 for 30 min, followed by incubation with 10% normal goat serum at room temperature for 60 min. The primary antibody is added and incubated at 4 °C for 16 h. After primary antibody incubation, the secondary antibody is incubated in the same manner for 2 h. DAPI (Biosharp) and F-actin (Thermo) are used to stain the nucleus and the cytoskeleton, respectively. All cells are observed and photographed with a Zeiss fluorescence microscope.

**Tissue IF assay:** Spinal cord specimens were cryo-embedded in optimal cutting temperature (OCT) compound and sectioned at 8- $\mu$ m thickness using a cryostat (Leica CM1950). Representative sections from each experimental group were randomly selected using a systematic random sampling protocol and subsequently processed using standardized IF protocols. Following antigen retrieval with citrate buffer (pH 6.0) and blocking with 5% normal goat serum, sections were incubated overnight at 4 °C with the following primary antibodies: anti-Nrf2 (Abcam), anti-GFAP (Proteintech), anti-CD31 (Santa Cruz Biotechnology), anti-Tuj1 (Abcam), and anti-NF200 (Santa Cruz Biotechnology). Corresponding species-matched Alexa Fluor-conjugated secondary antibodies (Abcam) were applied at 1:500 dilution for 2 h at room temperature. All sections were counterstained for nuclei with DAPI (Biosharp).

### Data analysis

Each experiment was conducted at least three times. Statistical analyses were performed using GraphPad Prism 8.0.2 software (San Diego, CA, USA). Data are presented as the mean  $\pm$  SD. Statistical differences between groups were analyzed by one-way analysis of variance (ANOVA) followed by Tukey's post hoc test. BBB scores were analyzed by repeated Two-way ANOVA and Tukey's post hoc test. A p-value less than 0.05 was considered statistically significant.

## Results

### Identification of hUC-MSCs

In this study, we prepared CS and CS-TP using hUC-MSCs. Inverted microscopy observations showed that hUC-MSCs exhibit a typical fibroblast-like morphology with spindle and polygonal shaped cells (Fig. 1A). At higher densities, they appear as relatively uniform spindle-shaped cells with a nested growth pattern. Flow cytometry indicated that hUC-MSCs strongly express stem cell surface markers: CD29, CD44, CD105, CD90

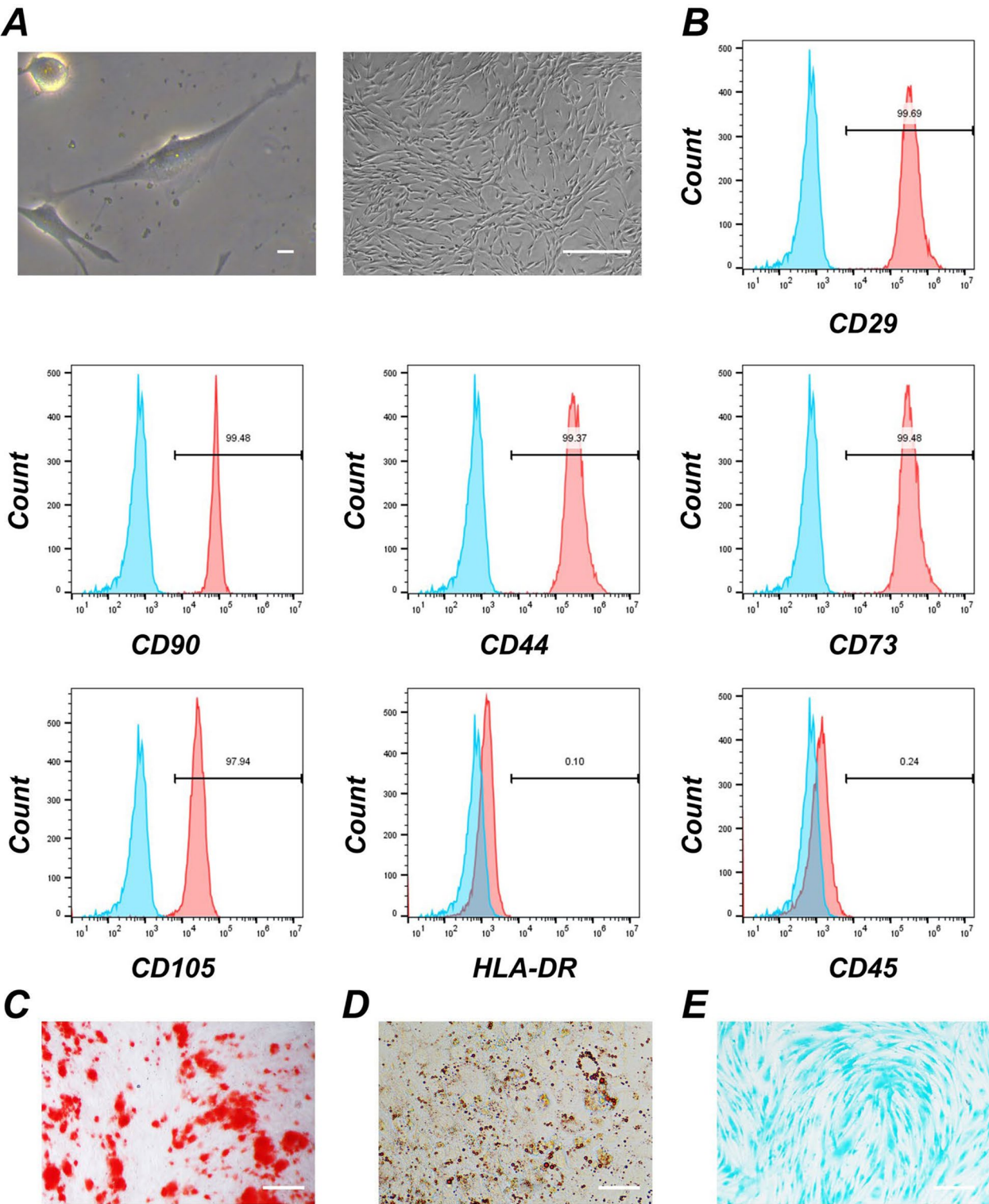


**Fig. 1** Morphology and characterization of hUC-MSCs. **A** Representative optical microscopy images of hUC-MSCs. Individual cell with fibroblast-like morphology (left) and high-density parallel or vortex morphology (right). **B** Flow cytometric analysis of surface markers of hUC-MSCs. **C–E** hUC-MSCs exhibited multi-lineage differentiation capability towards osteogenic, adipogenic, and chondrogenic lineages. Scale bars: 100  $\mu$ m (**A**); 200  $\mu$ m (**C, E**); 50  $\mu$ m (**D**)

and CD73 (>97% positive), but express low levels of HLA-DR and CD45 (<1% positive) (Fig. 1B). Oil Red O (Fig. 1C), Alizarin Red S (Fig. 1D), and Alcian Blue staining (Fig. 1E) demonstrated that hUC-MSCs can be differentiated into adipocytes, osteoblasts and chondrocytes in a multipotent manner.

#### Screening of TP concentration and characterization of CS and CS-TP

To ensure that TP does not inhibit the hUC-MSCs inherently present in CS and to maintain their normal viability, it is necessary to screen the concentration of TP by setting different concentration gradients and adding them to the culture medium of CS-TP. The cell viability in CS and CS-TP was measured using a CCK-8 kit on days 3, the results showed that a TP concentration of 5  $\mu$ M did not significantly inhibit the cells contained in CS (Fig. 2A). The test results from day 5 also demonstrate this conclusion (Fig. 2B). The hUC-MSCs formed dense CS, and the detached CS was soft in texture, while CS-TP was relatively hard and opaque.

HE and IF staining showed the positional relationship between nuclei and ECM. Additionally, the results of Collagen I staining indicated that both CS and CS-TP contained a large amount of collagen fibers. Scanning electron microscopy revealed that the CS surface was smooth and flat, whereas the CS-TP surface had fibrous filaments attached (Fig. 2C).

#### The protective effect on H<sub>2</sub>O<sub>2</sub>-induced PC12 cells and HUVECs

Live/dead staining results showed that after treating cells with CS and CS-TP for 3 days, a higher number of dead cells appeared in the H<sub>2</sub>O<sub>2</sub> group, while both CS and CS-TP promoted the survival of PC12 cells and HUVECs under high oxidative stress conditions. The protective effect of CS-TP on cells was more evident, significantly reducing the number of dead HUVECs and PC12 cells (Fig. 3A, D). The CCK-8 assay results were consistent with the above findings (Fig. 3B, C).

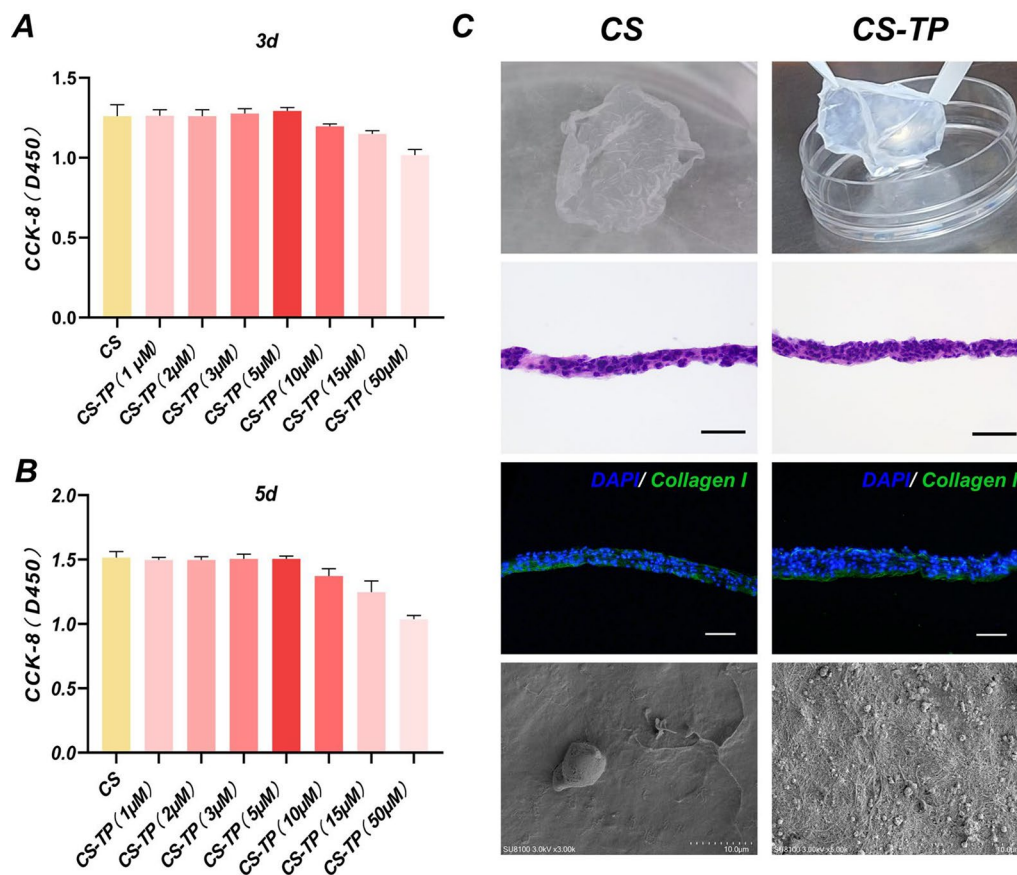


**Fig. 2** Screening of TP concentration and characterization of CS and CS-TP. **A** The effect of different concentrations of TP on cell viability in CS over 3 days. **B** The effect of different concentrations of TP on cell viability in CS over 5 days. **C** Characterization of CS and CS-TP. Scale bars: 200  $\mu$ m (C). Results are reported as mean  $\pm$  standard deviation (n = 3) \*p < 0.05, \*\*p < 0.01 and \*\*\*p < 0.001



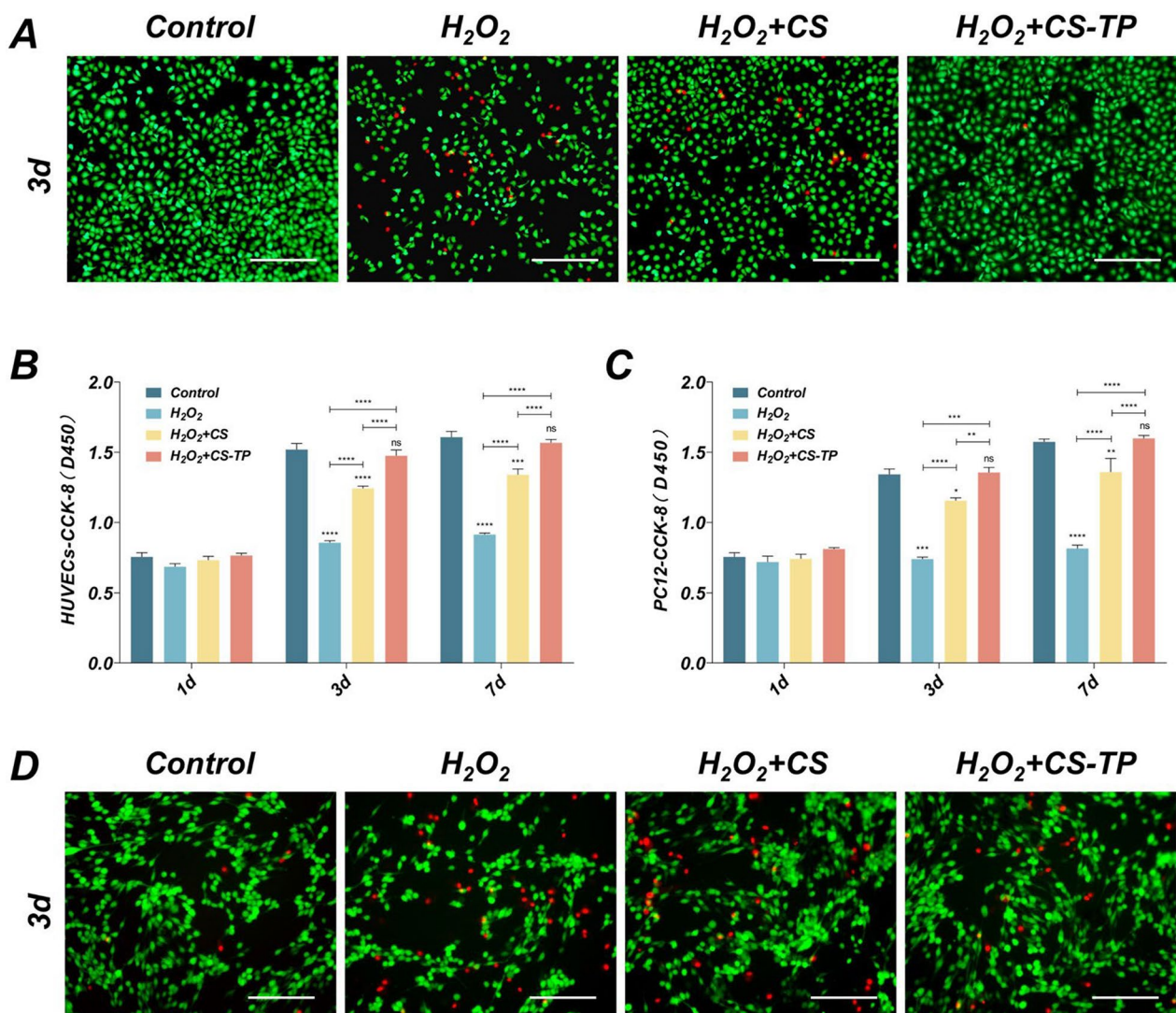


**Fig. 3** CS and CS-TP protect cell survival from oxidative stress conditions. **A** Fluorescence images of HUVECs stained with live/dead assay. **B** Cell viability of HUVECs detected by CCK-8 assay. **C** Cell viability of HUVECs detected by CCK-8 assay. **D** Fluorescence images of HUVECs stained with live/dead assay. Scale bars: 200  $\mu$ m (**A**, **C**). Results are reported as mean  $\pm$  standard deviation ( $n=3$ ) \* $p < 0.05$ , \*\* $p < 0.01$  and \*\*\* $p < 0.001$

### Reduced the production of cellular ROS in vitro

In a high oxidative stress environment, the level of cellular ROS is significantly elevated. ROS refers to a series of highly reactive oxygen-containing molecules, including superoxide anions, hydrogen peroxide, and hydroxyl radicals. When the production and accumulation of ROS exceed the cell's own antioxidant and defense capabilities,

it leads to cellular damage [30]. To assess whether CS and CS-TP can generate ROS in a high oxidative stress microenvironment, we used DCFH-DA flow cytometry to detect ROS levels in HUVECs and found that the ROS levels in the CS group showed a decreasing trend compared to the  $H_2O_2$  group, with the CS-TP group showing an even more pronounced decrease (Fig. 4A, B).

(See figure on next page.)

**Fig. 4** Reduced the production of cellular ROS in vitro. **A** Intracellular ROS levels in HUVECs of each group were determined using the DCFH-DA assay. **B** Quantitative analysis of ROS levels in HUVECs. **C** Representative fluorescence images of DCFH-DA in HUVECs. **D** Statistical analysis of DCFH-DA fluorescence intensity in HUVECs. **E** Intracellular ROS levels in PC12 cells of each group were determined using the DCFH-DA assay. **F** Statistical analysis of DCFH-DA fluorescence intensity in PC12 cells. Scale bars: 100  $\mu$ m (**C**); 200  $\mu$ m (**E**). Results are reported as mean  $\pm$  standard deviation ( $n=3$ ) \* $p < 0.05$ , \*\* $p < 0.01$  and \*\*\* $p < 0.001$

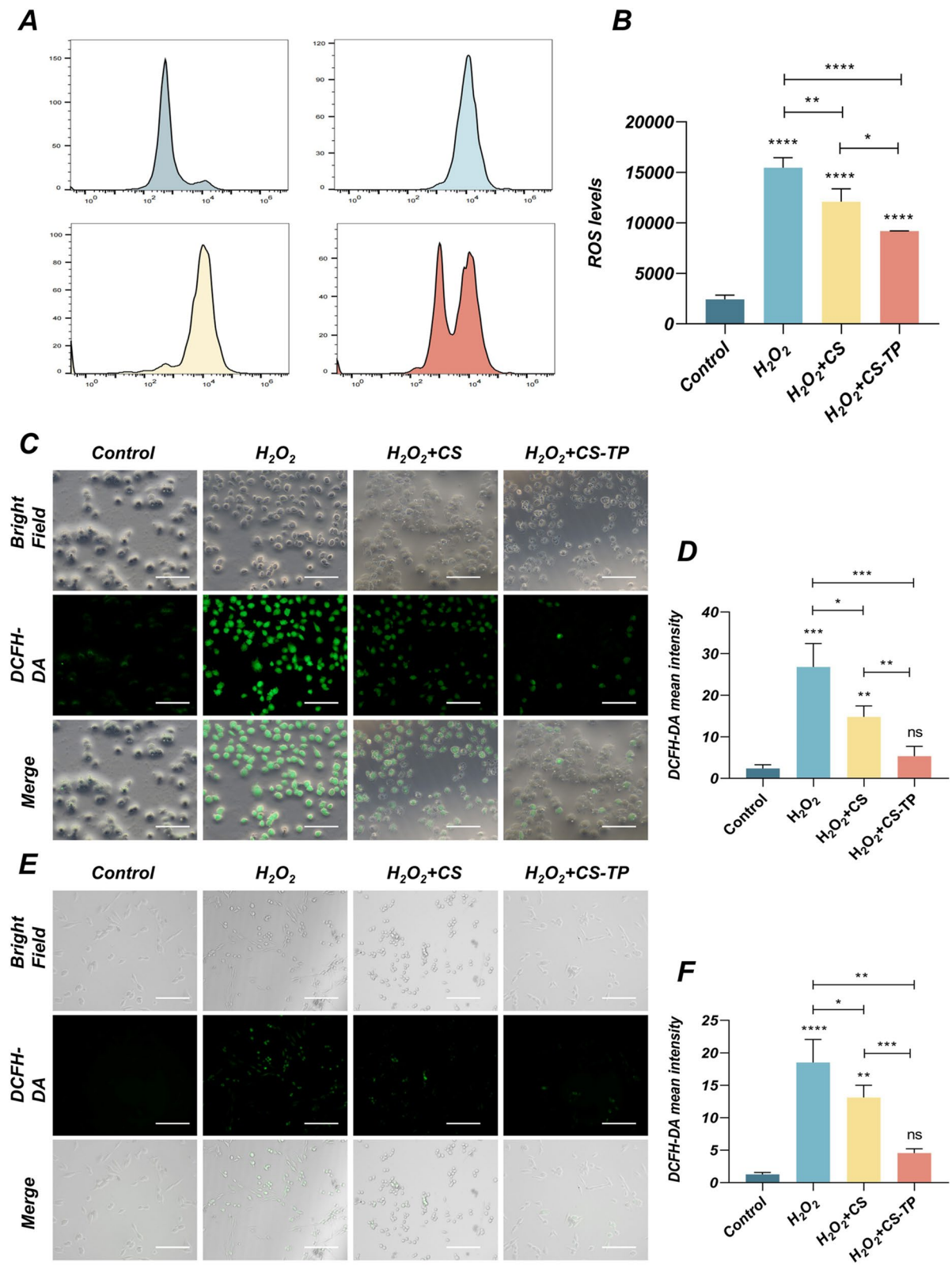


**Fig. 4** (See legend on previous page.)

The DCFH-DA fluorescence staining of HUVECs and PC12 cells also showed the same results (Fig. 4C–F). The green fluorescence intensity of cells in the  $H_2O_2$  group significantly increased, while the fluorescence intensity within cells decreased significantly after CS-TP treatment, indicating that CS-TP has a strong ROS scavenging capability.

#### **Promote Nrf2 nuclear translocation, downregulate Keap-1 protein, and upregulate HO-1 protein expression**

To further understand the molecular mechanisms by which CS and CS-TP counteract oxidative stress in PC12 cells and HUVECs, the transcription factor Nrf2 was studied as a potential regulator of the cellular antioxidant system. The classical activation pattern of Nrf2 involves its translocation from the cytoplasm to the nucleus. Therefore, we first investigated the accumulation of Nrf2 protein in the nucleus of cells treated with CS and CS-TP. Immunofluorescence confirmed the nuclear translocation of Nrf2 in PC12 cells and HUVECs. The results showed that CS and CS-TP promoted the nuclear translocation of Nrf2, subsequently activating Nrf2, with the effect of CS-TP being more pronounced. In the Control group and the  $H_2O_2$  group, Nrf2 was primarily located in the cytoplasm, whereas in cells treated with CS and CS-TP, Nrf2 translocated from the cytoplasm to the nucleus (Figs. 5A, 6A). The results of Western blotting analysis showed that after treatment with CS and CS-TP, Nrf2 significantly increased in the nucleus, and there was a decreasing trend of Nrf2 in the cytoplasm (Figs. 5B–D, 6B–D). Therefore, we hypothesized that CS and CS-TP might regulate the upstream and downstream target genes of Nrf2, and we examined the protein expression of the upstream factor Keap-1 and the downstream factor HO-1 in this pathway. The results demonstrated that Keap-1 protein was significantly upregulated in the  $H_2O_2$  group, while the upregulation of Keap-1 was markedly reduced after treatment with CS and CS-TP. Additionally, compared to the Control group and the  $H_2O_2$  group, CS and CS-TP enhanced the expression of HO-1 protein (Figs. 5E–G, 6E–G). These results suggest that CS and CS-TP induce the protein expression of the upstream factor Keap-1 and the downstream factor HO-1 by activating the Nrf2 signaling pathway.

#### **Promotion of HUVECs biological behavior induced by $H_2O_2$ in vitro**

In order to investigate whether CS and CS-TP can improve the functional recovery of HUVECs under  $H_2O_2$ -induced oxidative stress, several biological behavior assays were conducted, as shown in Fig. 7A. Statistical results show that, compared to the  $H_2O_2$  group, CS and CS-TP treatment led to an increase in

the migration rate of HUVECs (Fig. 7B) and a higher number of invasions (Fig. 7C). Additionally, the Matrigel tube formation assay is an in vitro model of angiogenesis. When the CS and CS-TP groups were added to HUVECs treated with  $H_2O_2$ , more capillary-like structures were observed. Quantitative measurements showed that the total tube length, total branch points, and total loops in the CS-TP group were significantly higher than those in the  $H_2O_2$  group and CS group, while the difference with the Control group became smaller (Fig. 7D–G). These findings suggest that CS-TP can effectively enhance the functional recovery of HUVECs under  $H_2O_2$ -induced oxidative conditions.

#### **Improvement of motor function recovery after SCI in rats**

To evaluate the impact of CS and CS-TP on the recovery of motor function after SCI, approximately a 2 mm injury was inflicted on the left side of the spinal cord in rats (Fig. 8A). The BBB scores were used to assess the recovery of motor function after SCI at specific postoperative times for each group of rats (Fig. 8B). Before the surgery, each rat exhibited a typical motor function in the left hind limb (21 points). After the left spinal cord hemisection, the rats showed complete paralysis of the left hind limb (0 points). A statistically significant difference was observed between the CS group and the SCI group 2–4 weeks after surgery. CS-TP may have a positive effect on the restoration of rats' motor function after SCI in the early stage, and this advantage lasts until the late stage. At four weeks post-surgery, most of the rats that received CS-TP implantation exhibited sustained palm-supporting movement and coordinated forelimb and hindlimb movement, with scores ranging from 12 to 16 points. Similarly, most rats in the CS group exhibited supported palm-supporting movement and coordinated forelimb and hindlimb movement, with scores ranging from 10 to 14 points. Rats with SCI only exhibited ankle joint movement (6–8 points). These findings strongly support the notion that CS-TP accelerates functional recovery after SCI.

Footprint analysis showed similar BBB scores results (Fig. 8C). Four weeks after SCI, rats in the SCI group exhibited only left hindlimb dragging. Rats treated with CS demonstrated good forelimb and hindlimb coordination, but the gait trajectory of the left hindlimb was inconsistent. In contrast, the CS-TP group exhibited more coordinated forelimb-hindlimb movements. There was no significant difference in stride length and average intensity between the CS-TP group and the sham surgery group (Fig. 8D–F). These findings suggest that CS-TP treatment improved motor function in rats.



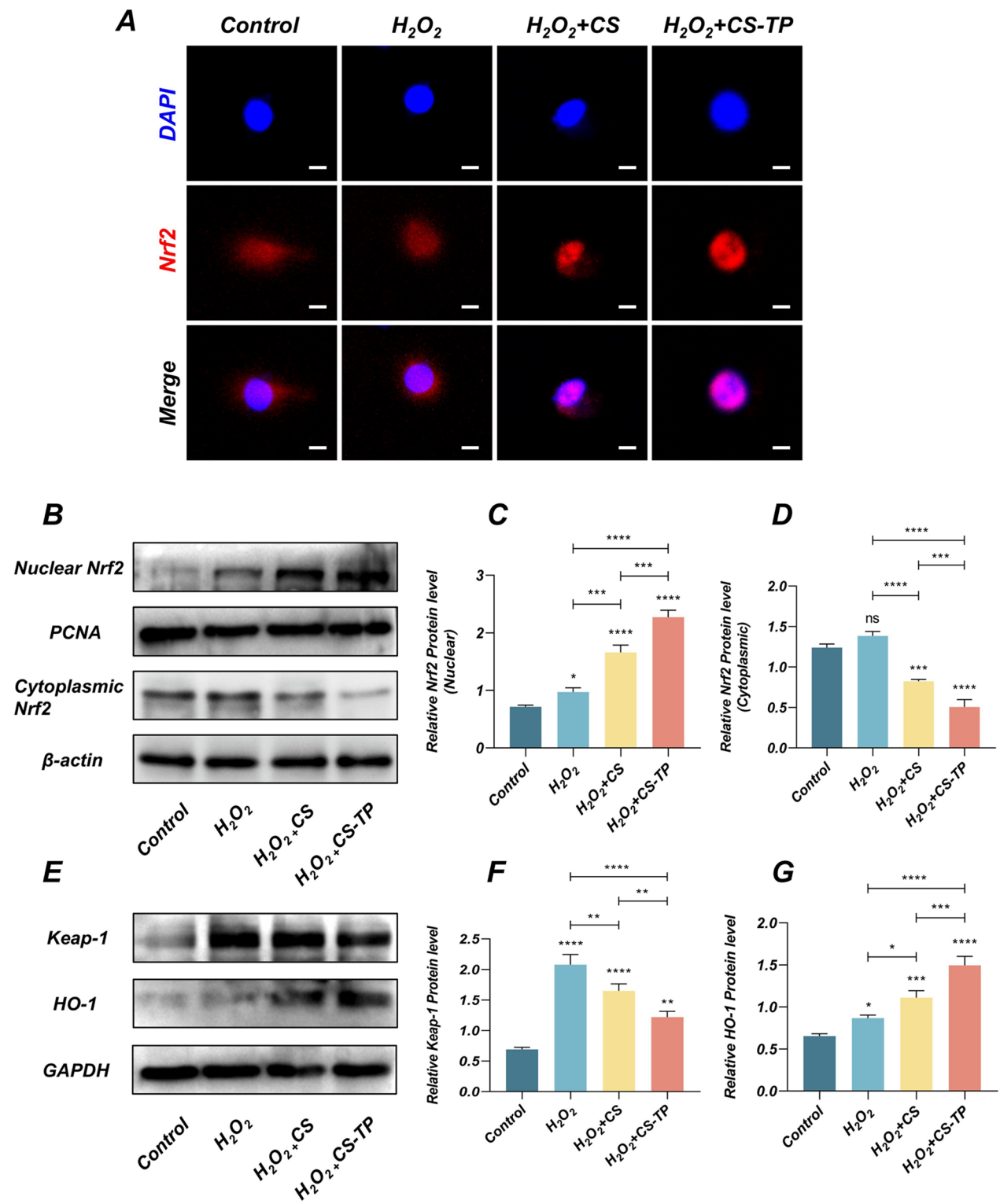


**Fig. 5** CS and CS-TP activate the Keap-1/Nrf2/HO-1 signaling pathway in PC12 cells. **A** IF images using anti-Nrf2 antibodies show the nuclear translocation of Nrf2 in PC12 cells treated with CS and CS-TP. **B** Analysis by Western blotting of the levels of Nrf2 protein in the cytoplasm and nucleus of PC12 cells. **C** Quantitative analysis of Nrf2 protein levels in the nucleus. **D** Quantitative analysis of Nrf2 protein levels in the cytoplasm. **E** Keap-1 and HO-1 protein levels in PC12 cells analyzed by Western blotting. **F** Quantitative analysis of Keap-1 protein levels. **G** Quantitative analysis of HO-1 protein levels. Scale bars: 20 μm (**A**). Results are reported as mean ± standard deviation (n = 3) \*p < 0.05, \*\*p < 0.01 and \*\*\*p < 0.001

### Activates the Keap-1/Nrf2/HO-1 signaling pathway in SCI rats

The Keap-1/Nrf2/HO-1 pathway as one of the major antioxidant pathways, which is a key step in cellular/tissue protection from oxidative damage [31–34]. To explore whether this pathway is activated after the implantation of CS and CS-TP. First, we assessed the content of Nrf2 by histological fluorescence staining (Fig. 9A, B), and the results showed that both CS and CS-TP implantation increased the content of Nrf2, which was more obvious in the CS-TP group. TP are rich in various bioactive components, including flavonoids and polyphenols. Prior research has established that EGCG is the predominant constituent of TP, representing the largest proportion among its components, and is crucial for the antioxidant activity exhibited by TP [35]. Consequently, we have chosen EGCG as a molecular model to investigate its potential affinity with Nrf2 within the context of TP. Molecular docking studies helped to validate the potential interactions between CS-TP and proteins in the Keap-1/Nrf2/HO-1 pathway. Docking results showed that the binding energies were  $-7.1$  kcal/mol and  $-9$  kcal/mol, respectively, indicating that the compound has considerable binding potential to its protein targets due to the low energy association (Fig. 9C). This provides evidence that EGCG may serve as the main bioactive component exerting antioxidant effects as TP and activating the Keap-1/Nrf2/HO-1 pathway. Western blot analysis further revealed the ability of CS-TP to induce Nrf2 nuclear translocation and enhance the expression of antioxidant enzymes HO-1, SOD1, and SOD2. These results suggested that CS-TP activated the Keap-1/Nrf2/HO-1 signaling pathway and enhanced the antioxidant capacity of cells after SCI (Fig. 9D–I). The Keap-1/Nrf2/HO-1 signaling pathway in the spinal cord of acute SCI rats.

### CS and CS-TP facilitate angiogenesis in vivo

Improvement of blood supply is closely associated with changes in the microenvironment of the injured zone. Intact vascular structure and sufficient blood supply could clear the local apoptotic cell debris and promote oxygen/nutrient transport, which are crucial for neural repair after SCI. Since CD31 is biomarker for endothelial cells, the vascular number after SCI can be quantified by IF for CD31. One week after surgery,

we performed IF staining for vascular marker CD31 (also known as platelet endothelial cells molecule-1 (PECAM-1)) in spinal cord tissues. The results showed that SCI group had the lowest expression of CD31, indicating the limited number of newly formed vessels. CS group had an increased expression of CD31 compared with the SCI group, suggesting that CS plays a role in promoting angiogenesis after SCI. Compared with SCI group and CS group, CS-TP group showed more CD31-positive vascular structures, which were much wider in distribution (Fig. 10A, B). The above results indicate that CS-TP could effectively promote angiogenesis after SCI.

### CS and CS-TP promote neuronal regeneration and axon extension in vivo

To further investigate the discrepancy between CS and CS-TP in promoting the histological changes and functional recovery of SCI, we likewise employed IF localization of regenerating neurons and axonal extension. Four weeks after the injury, a great number of Tuj-1 positive neurons were detected in the epicenter of SCI in CS and CS-TP groups, while the incidence of neuron was significantly lower in SCI group (Fig. 11A). The number of regenerated NF200 positive axons at the injury site was further quantified by measuring the optical density of regenerated NF200 negative axons. The results revealed that the mean fluorescence intensity of NF200 in the injury epicenter of CS and CS-TP groups was remarkably higher than that in other groups, whereas only a few NF200 positive axons were observed in the SCI and CS groups (Fig. 11C). Notably, the statistical results showed a minor difference between SCI and CS groups in Tuj-1 and NF200 (Fig. 11B, D). As the result mentioned above, CS-TP significantly promoted the regeneration of neurons and axonal extension.

To evaluate the safety of CS and CS-TP, various organs were stained with H&E. The results are shown in Fig. 12A. The CS and CS-TP are biocompatible and have no significant effects on general tissues. The pathological examinations of the heart, liver, spleen, lung and kidney in all groups were basically the same and no significant abnormalities were found, which proved this fact.

(See figure on next page.)

**Fig. 6** CS and CS-TP activate the Keap-1/Nrf2/HO-1 signaling pathway in HUVECs. **A** IF images using anti-Nrf2 antibodies show the nuclear translocation of Nrf2 in HUVECs treated with CS and CS-TP. **B** Analysis by Western blotting of the levels of Nrf2 protein in the cytoplasm and nucleus of HUVECs. **C** Quantitative analysis of Nrf2 protein levels in the nucleus. **D** Quantitative analysis of Nrf2 protein levels in the cytoplasm. **E** Keap-1 and HO-1 protein levels in HUVECs analyzed by Western blotting. **F** Quantitative analysis of Keap-1 protein levels. **G** Quantitative analysis of HO-1 protein levels. Scale bars: 200  $\mu$ m (**A**). Results are reported as mean  $\pm$  standard deviation ( $n=3$ ) \* $p<0.05$ , \*\* $p<0.01$  and \*\*\* $p<0.001$

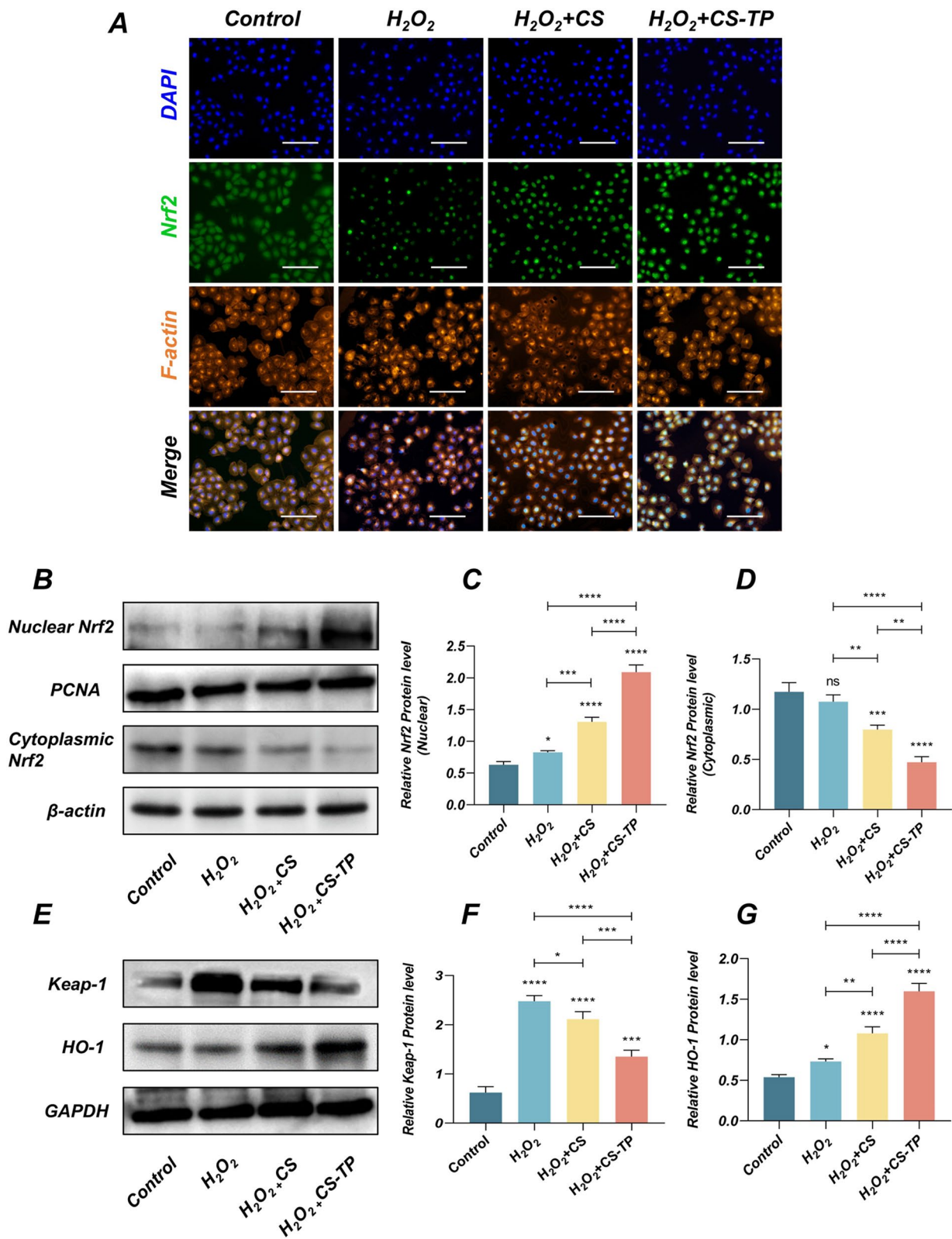


**Fig. 6** (See legend on previous page.)



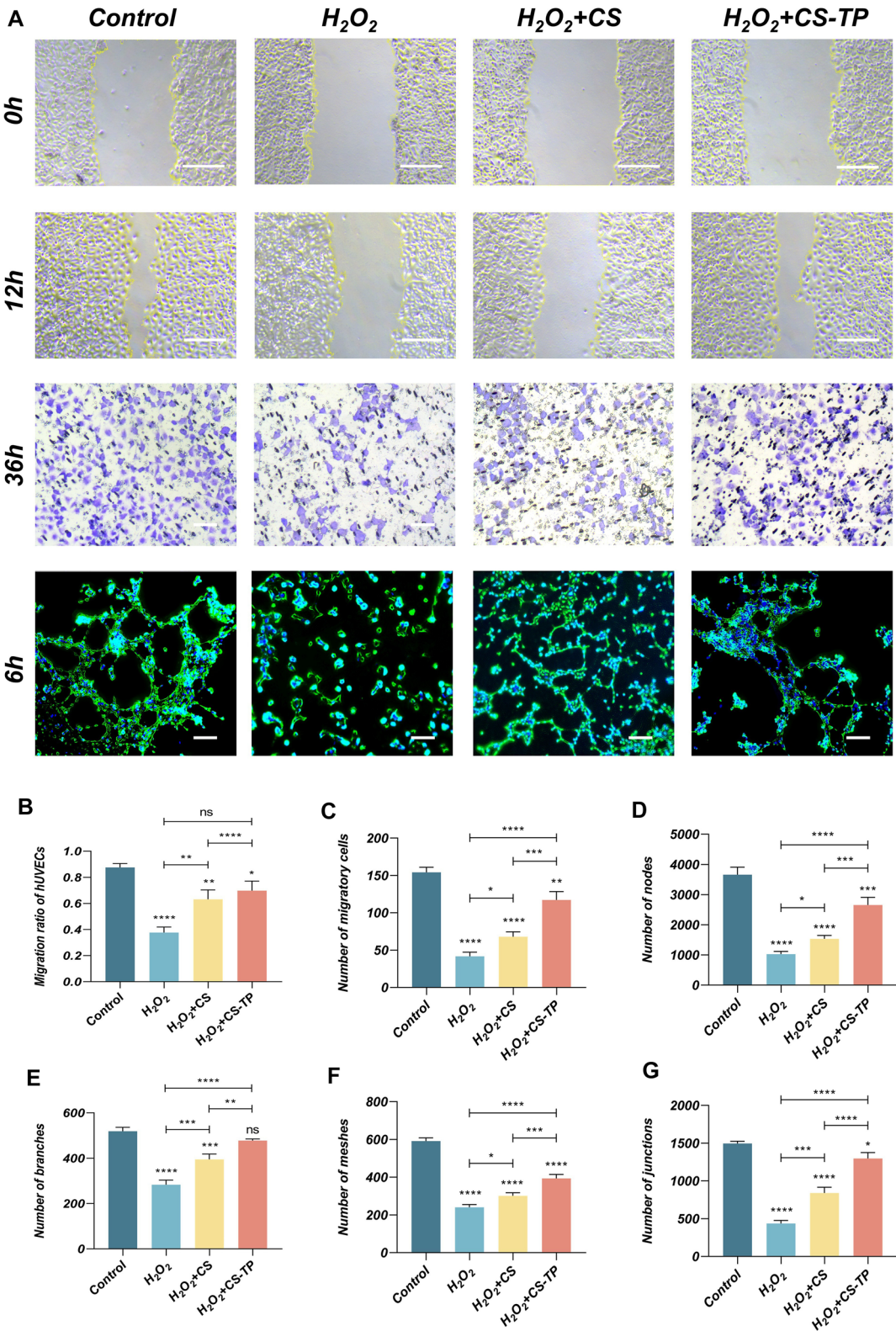


**Fig. 7** In vitro CS and CS-TP promote the biological behavior of HUVECs. **A** Effects on HUVECs migration; invasive capacity; representative tube formation images in each group. **B** Statistical migration ratio of HUVECs migration. **C** Effects migration quantification on the of HUVECs in each group. **D–G** Quantitative evaluation of capillary nodes, meshes, junctions, and branches in HUVECs after treatment with each group. Scale bars: 200  $\mu$ m (**A**). Results are reported as mean  $\pm$  standard deviation (n=3) \*p<0.05, \*\*p<0.01 and \*\*\*p<0.001

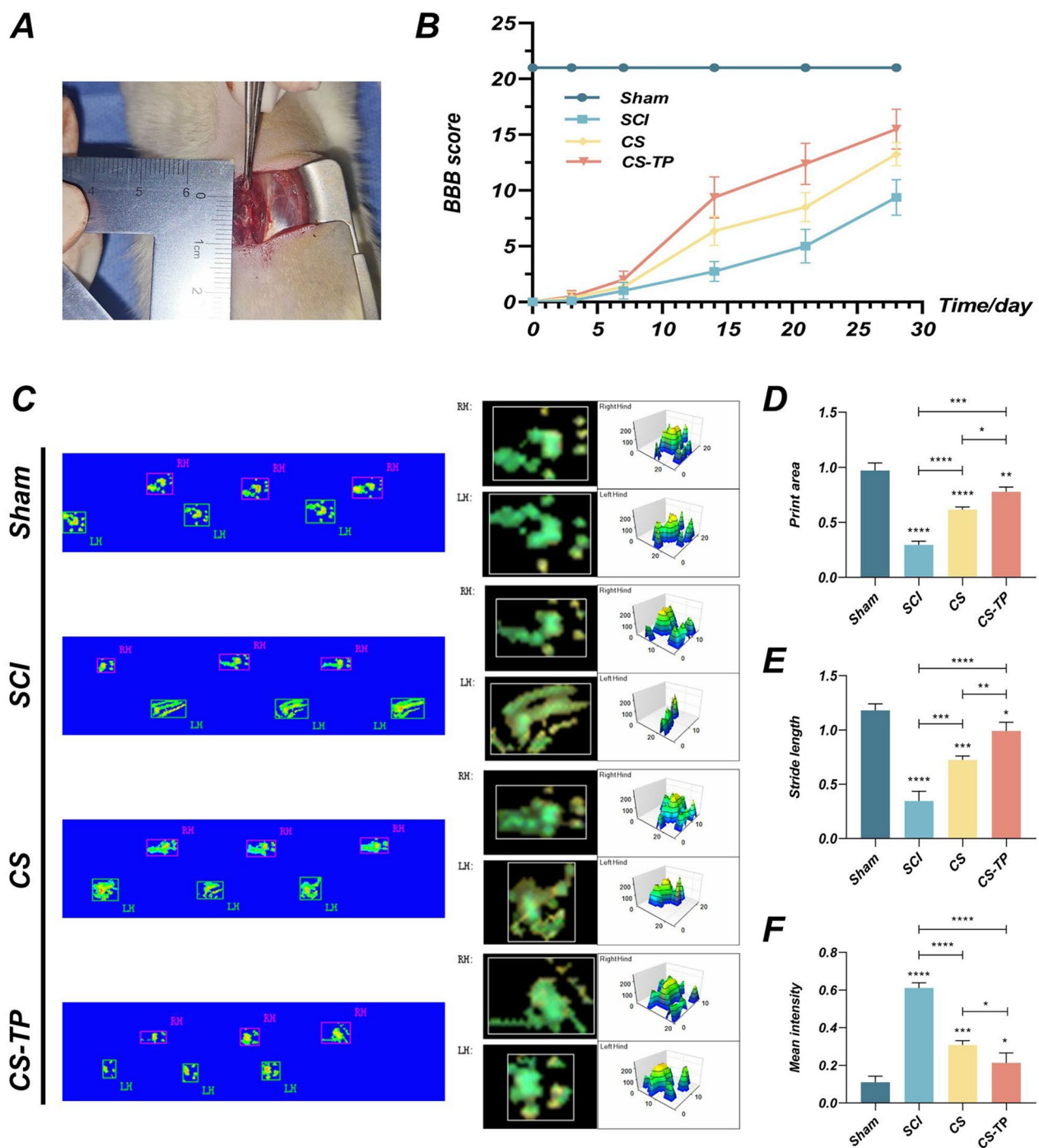


**Fig. 8** CS and CS-TP promote the recovery of motor function after SCI in rats. **A** Schematic diagram of the left spinal cord hemisection injury model in rats. **B** Left hind limb motor recovery was measured by BBB scores. **C** Representative footprints were used to analyze the recovery of hind limb motor function. **D–F** Quantification of print area, stride length, and mean intensity of the left hindlimb at 4 weeks after surgery in each group. Results are reported as mean  $\pm$  standard deviation ( $n=3$ ) \* $p < 0.05$ , \*\* $p < 0.01$  and \*\*\* $p < 0.001$

## Discussion

In this study, we prepared a more protective and regulatory CS-TP based on the foundation of CS. CS-TP retains

the advantages of CS itself while effectively enhancing its therapeutic effects (Fig. 13). Additionally, since we selected TP as the loading component, we explored the

molecular mechanism of CS-TP from the perspective of anti-oxidative stress.

The poor reparative ability of neurons and the secondary deterioration of the microenvironment are some of the main reasons why functional recovery is limited after SCI [30]. The improvement of blood supply is closely related to changes in the microenvironment of the injured area. Primary mechanical injury leads to the rupture of microvessels in the surrounding tissue and the destruction of the blood-spinal cord barrier (BSCB), which further leads to ischemia and hypoxia, resulting in pathological changes such as inflammatory cell infiltration and necrosis of neural tissue [36]. An intact vascular structure and abundant blood supply can clear locally apoptotic cell debris, and metabolic products, and promote the transport of oxygen/nutrients [36]. Therefore, the vascular system of the spinal cord plays a crucial role in the process of SCI and repair [37, 38]. Vascular endothelial cells, as the most important component of the vascular system, experience a significant loss in acute SCI. Therefore, in the treatment of patients with SCI, the generation of endothelial cells should be promoted as much as possible to aid in the reconstruction of blood supply and create a microenvironment conducive to nerve repair. However, the free radicals produced by oxidative stress after SCI change dramatically and are one of the main pathological factors of secondary injury in SCI, which can lead to endothelial dysfunction and reduced endogenous repair at the site of SCI [39, 40]. In the secondary injury phase of SCI, increased ROS production can activate mitochondria-mediated apoptosis signaling pathways, eventually leading to aggravated neuronal death and promoting lesion progression [41]. ROS are a major form of oxidants that can lead to lipid peroxidation, protein inactivation, and DNA fragmentation, ultimately resulting in cellular dysfunction or even death.

The use of MSCs for treatment is currently considered an effective strategy to promote vascular repair in spinal cord injuries, commonly through intramedullary or intravenous injection of cells [20, 42]. To better utilize the cells, we prepared CS using cell sheet technology to promote early angiogenesis in SCI. In this study, we used hUC-MSCs as the cell source for preparing cell sheet because hUC-MSCs can secrete a large amount

of pro-angiogenic factors and have been used in many ischemic diseases [43]. Previous studies have confirmed the efficacy and safety of using CS for treatment [44, 45]. Notably, the formation of cell sheet not only helps cells remain at the injury site for an extended period, but also significantly increases cell survival due to the presence of the extracellular matrix (ECM) [46]. Additionally, ECM provides a natural scaffold for cell and tissue regeneration, connecting both ends of the SCI and effectively filling the defect.

TP is a safe, biocompatible plant-derived polyphenol that has been approved by the FDA and holds tremendous clinical potential for the advancement of biomedicine [47]. TP is rich in phenolic hydroxyl groups and exhibits excellent antioxidant and anti-inflammatory properties [48]. Furthermore, TP can modify and enhance various materials, including collagen, chitosan, and cellulose, through hydrogen bonding, and is widely applied in the biomedical field. CS contains abundant ECM components, including fibrin and collagen [24, 45], which provide potential for binding with TP. Therefore, this study achieved the combination of TP with CS through a simple method to prepare CS-TP, enhancing the oxidative stress resistance of CS and reducing the production of cellular ROS. Subsequently, the functionality and biocompatibility of CS-TP were evaluated, both demonstrating favorable results. In exploring how much TP content CS can specifically load and release, we have found that under current conditions, the combination and release of TP and CS is limited, which may restrict the therapeutic effect of CS-TP to some extent. In response to this issue, we hope to optimize their combination method in future research to maximize the therapeutic effect of CS-TP.

In vitro, we co-incubated endothelial cells with CS and CS-TP separately. The experimental results showed that compared to CS, CS-TP effectively reduced the production of ROS in HUVECs and PC12 cells, significantly improved cell survival under H<sub>2</sub>O<sub>2</sub>-induced oxidative stress damage. This indicates that CS-TP could resist oxidative stress, favoring the survival of endothelial cells and neural cells in adverse microenvironments. Additionally, to better elucidate the intrinsic mechanisms by which CS and CS-TP promote endothelial cell and neuron repair,

(See figure on next page.)

**Fig. 9** CS and CS-TP could activate the Keap-1/Nrf2/HO-1 signaling pathway in SCI spinal cord tissues. **A** IF imaging of Nrf2 (red) antibody was used to evaluate the Nrf2 content in the lesion site of all groups 1 week after the surgery in rats. **B** Quantitative analysis of the Nrf2 positive staining area. **C** Molecular docking results. **D** Protein expression levels of Keap-1/Nrf2/HO-1 in the spinal cord tissues one week after surgery. **E** Quantitative analysis results of Keap-1. **F** Quantitative analysis results of Nrf2. **G** Quantitative analysis results of HO-1. **H** Quantitative analysis results of SOD1. **I** Quantitative analysis results of SOD2. Scale bars: 200  $\mu$ m (**A**). Results are reported as mean  $\pm$  standard deviation (n = 3) \*p < 0.05, \*\*p < 0.01 and \*\*\*p < 0.001



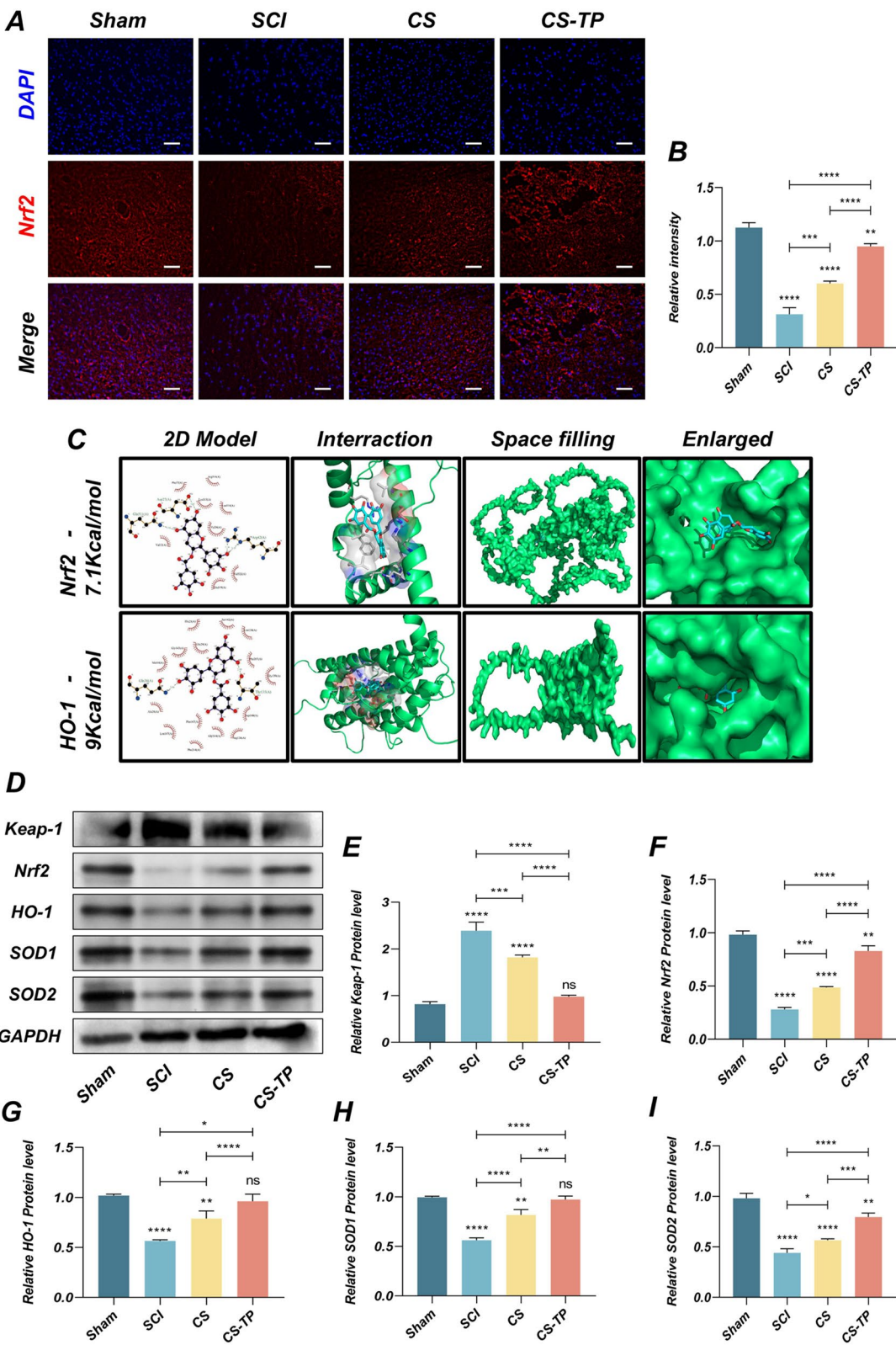


**Fig. 9** (See legend on previous page.)

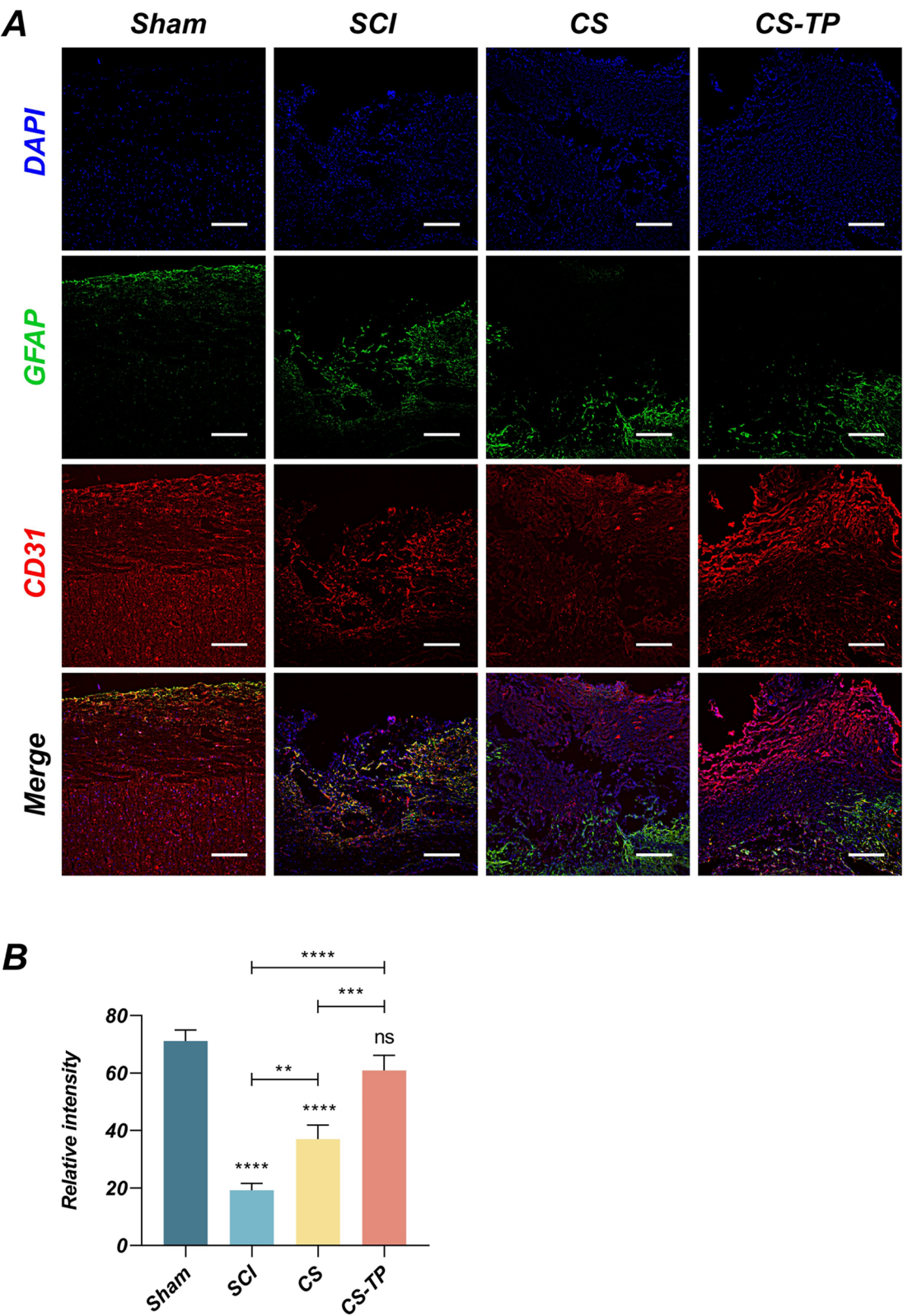


**Fig. 10** Angiogenesis in vivo promoted by CS and CS-TP after 1 week. **A** Angiogenesis was assessed in all groups at a lesion site by IF imaging using GFAP (green) and CD31 (red) antibodies. **B** Quantitative analyses of the CD31-positive staining area. Scale bars: 100  $\mu$ m (**A**). Results are reported as mean  $\pm$  standard deviation (n = 3) \*p < 0.05, \*\*p < 0.01 and \*\*\*p < 0.001

we verified this using immunofluorescence staining and Western blot experiments. Given that CS and CS-TP effectively protect the survival of  $H_2O_2$ -induced PC12 cells and HUVECs, and the intracellular ROS levels are significantly reduced, we hypothesize that they may be involved in the cellular antioxidant response. Nrf2 is an important mediator expressing antioxidant enzymes and stress-inducible proteins. The activation of the Nrf2/Keap-1/HO-1 signaling pathway is crucial for reducing cellular damage and regulating oxidative stress [49]. Under non-oxidative conditions, Nrf2 binds with Keap-1 to form a complex, which is sequestered within the cell. Under certain conditions, such as post-oxidation, Nrf2 separates from the Keap-1-Nrf2 complex, transfers to the nucleus, and enhances the cellular response to oxidative stress [50]. Based on this, we used immunofluorescence staining to observe the nuclear translocation of Nrf2 in PC12 cells and HUVECs. The results showed that both CS and CS-TP can promote the accumulation of Nrf2 in the nucleus and enhance its expression. After oxidation, the complex composed of Nrf2 and Keap-1 separates and transfers to the nucleus, combines with HO-1, and enhances the cellular response to oxidative stress [51]. Numerous pieces of evidence indicate that HO-1 plays an important role in cellular protection functions against oxidative damage. Upregulation of HO-1 and response to oxidative stress provides an effective endogenous antioxidant defense mechanism [52]. Subsequent Western blot data showed that CS and CS-TP promoted the translocation of Nrf2 from the cytoplasm to the nucleus, indicating that Nrf2 was activated. Simultaneously, the HO-1 protein level also increased. Overall, these results suggest that CS and CS-TP improve the damage to PC12 cells and HUVECs induced by  $H_2O_2$  by activating the Keap-1/Nrf2/HO-1 signaling pathway. To assess the indirect effects of CS-TP on the biological behavior of vascular Endothelial cells, scratch and tube formation assays were conducted. The results showed that both CS and CS-TP could promote the migration of HUVECs and the formation of a two-dimensional capillary-like tubular structure, with the therapeutic effect of CS-TP being more pronounced.

In vivo experiments, to investigate the specific mechanism of action of CS-TP implantation in rats, we performed Nrf2 staining, molecular docking, and related

protein detection in rat spinal cord tissue sections. Current results indicate that both CS and CS-TP implantation significantly inhibit Keap-1 expression after spinal cord injury (SCI) and increase the protein expression of Nrf2 and HO-1. The promoting effect of CS-TP is more significant. Furthermore, both CS and CS-TP also lead to the upregulation of the antioxidant proteins SOD1 and SOD2, further demonstrating their antioxidant effects. Notably, CS-TP shows a marked improvement in therapeutic effect compared to CS. As the difference between the two lies in the loading of TP, we speculate that this more pronounced therapeutic effect originates from TP. As a natural polyphenol/flavonoid hybrid, the bioactive components in TP exhibit remarkable diversity, primarily comprised of catechins such as EGCG and epicatechin gallate (ECG), and flavonoids such as quercetin and kaempferol [53]. It is worth noting that EGCG stands out as the predominant component with the highest content proportion [54]. Previous studies have consistently shown that EGCG in TP has a significant antioxidant effect [55]. Therefore, in this study, we propose that EGCG in TP may exert its antioxidant effects via activation of the Keap-1/Nrf2/HO-1 pathway. The molecular structure of EGCG features multiple phenolic hydroxyl groups, which confer strong antioxidant properties by scavenging free radicals and activating the Nrf2/ARE antioxidant defense pathway [56]. Moreover, EGCG demonstrates potent anti-inflammatory activity through the regulation of signaling pathways such as NF- $\kappa$ B and MAPK, effectively inhibiting the release of pro-inflammatory cytokines like IL-6 and TNF- $\alpha$  [35]. In recent years, advancements in drug-delivery systems and structural modifications have opened new avenues for its clinical application. In the molecular docking process, we selected the rat as the species for simulation and tested the docking of EGCG (molecular formula:  $C_{22}H_{18}O_{11}$ ; molecular weight: 458.372) with Nrf2 and HO-1. The simulation results show that EGCG has a strong affinity for Nrf2 and HO-1, further supporting the enhancing effect of TP loading on CS and suggesting that EGCG may be the primary source for effectively activating the Keap-1/Nrf2/HO-1 pathway.

Determine the angiogenesis in spinal cord defect area of rats treated with CS and CS-TP. We used CD31 IF to label the local injury and found significant angiogenesis

(See figure on next page.)

**Fig. 11** Neuronal regeneration and axon elongation in vivo are promoted 4 weeks after CS-TP treatment. **A** Neuronal growth was assessed by IF imaging with GFAP (green) and Tuj-1 (red) antibodies in all groups at the lesion site. **B** Statistical graphs quantifying the relative fluorescence intensity of Tuj-1. **C** Axonal regeneration was assessed by IF imaging with GFAP (green) and NF200 (red) antibodies in all groups at the lesion site. **D** Statistical graphs quantifying the relative fluorescence intensity of NF200. Scale bars: 100  $\mu$ m (**A**, **C**). Results are reported as mean  $\pm$  standard deviation (n = 3) \*p < 0.05, \*\*p < 0.01 and \*\*\*p < 0.001



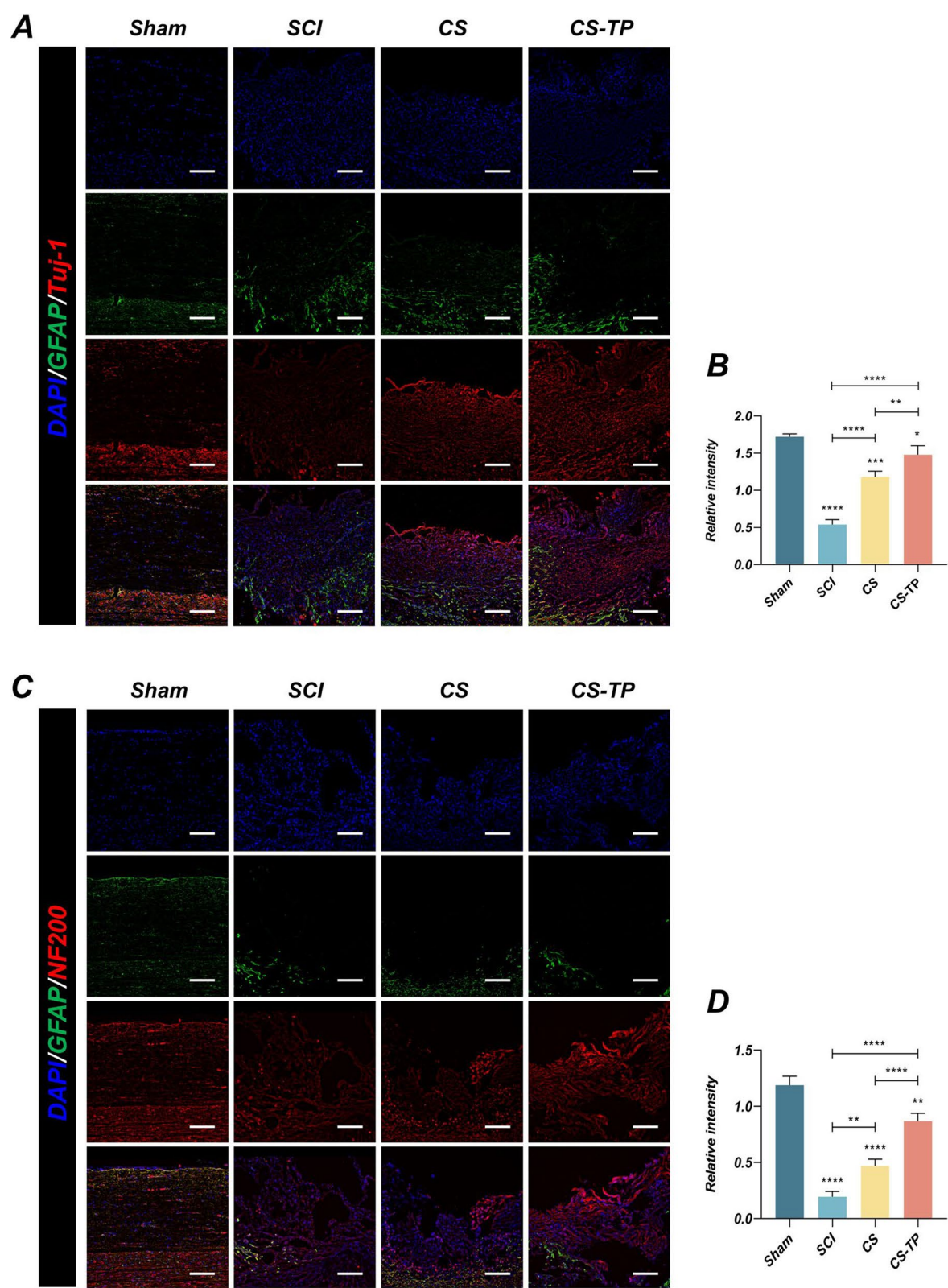


**Fig. 11** (See legend on previous page.)

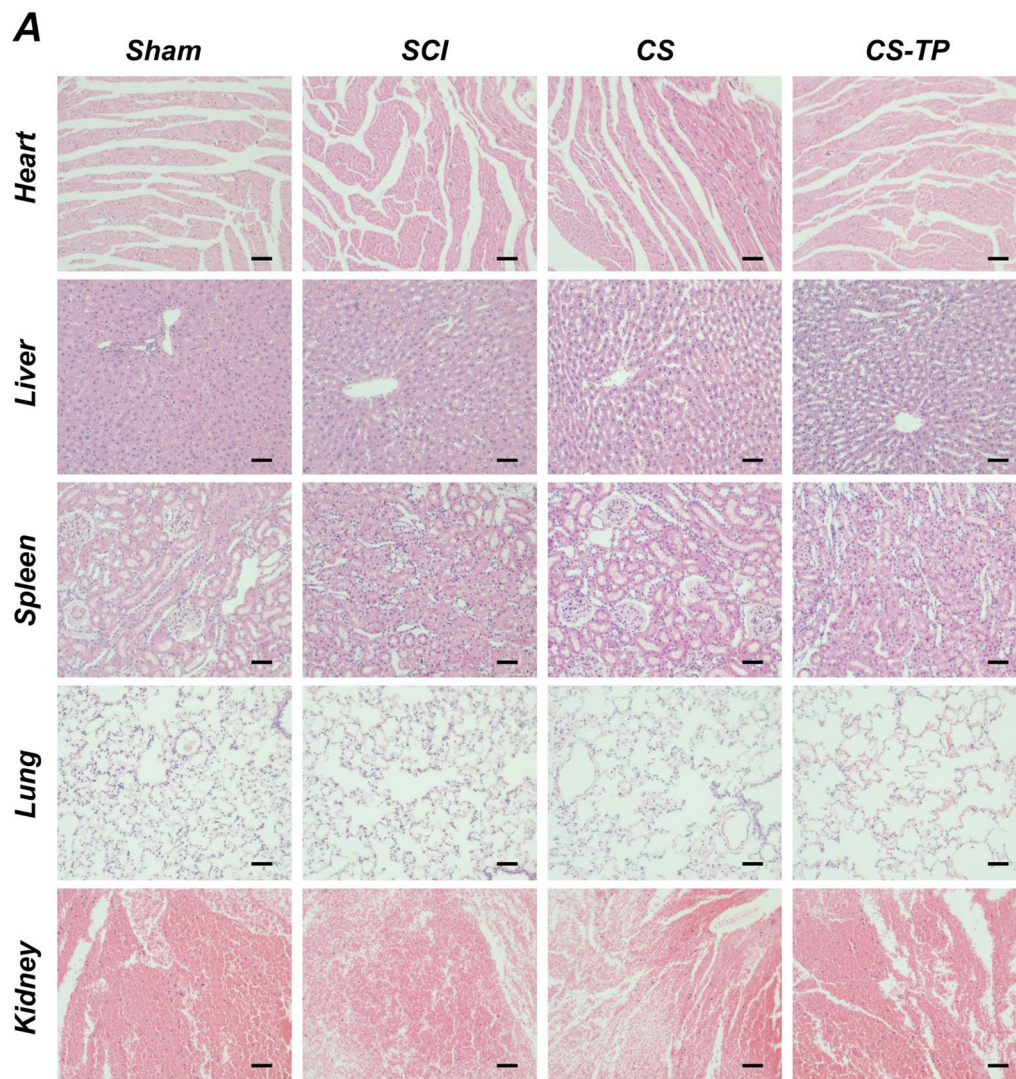


**Fig. 12** CS and CS-TP implants showed no *in vivo* tissue toxicity. **A** H&E staining of heart, liver, spleen, lung, and kidney from each group of rats. Scale bars: 200 μm (**A**)

in both the CS and CS-TP groups, with the repair effect being more pronounced in the CS-TP group. In terms of nerve repair, the staining results of Tuj-1 and NF200 also demonstrate that the implantation of CS-TP has a positive effect. Gait analysis results also supported these conclusions. Rats in the CS-TP group showed normal gait coordination four weeks after SCI, with the left hind limb actively supporting body weight. In contrast, only ankle joint movements were observed in the SCI group. CS-TP promoted the recovery of motor function. It is evident that, whether *in vitro* or *in vivo* experiments, CS has a certain therapeutic effect; however, the effect of CS-TP is more evident, suggesting that using CS-TP to promote SCI repair may be a more ideal approach.

## Conclusion

In conclusion, CS-TP promotes SCI repair from multiple aspects. Our current research aims to improve it while retaining the original functions of CS, enabling it to perform more effectively. The results demonstrate that CS-TP retains and enhances the biological functions of CS, compensating for the limitations of CS in adverse microenvironments. The loading of TP can effectively activate the Keap-1/Nrf2/HO-1 pathway, significantly enhancing the antioxidant stress ability of CS, aligning with the initial intention of our research strategy design. The core concept of sequential stem cell transplantation therapy is to repair and supplement the adverse microenvironment following SCI. CS-TP has effectively undertaken this task, significantly promoting



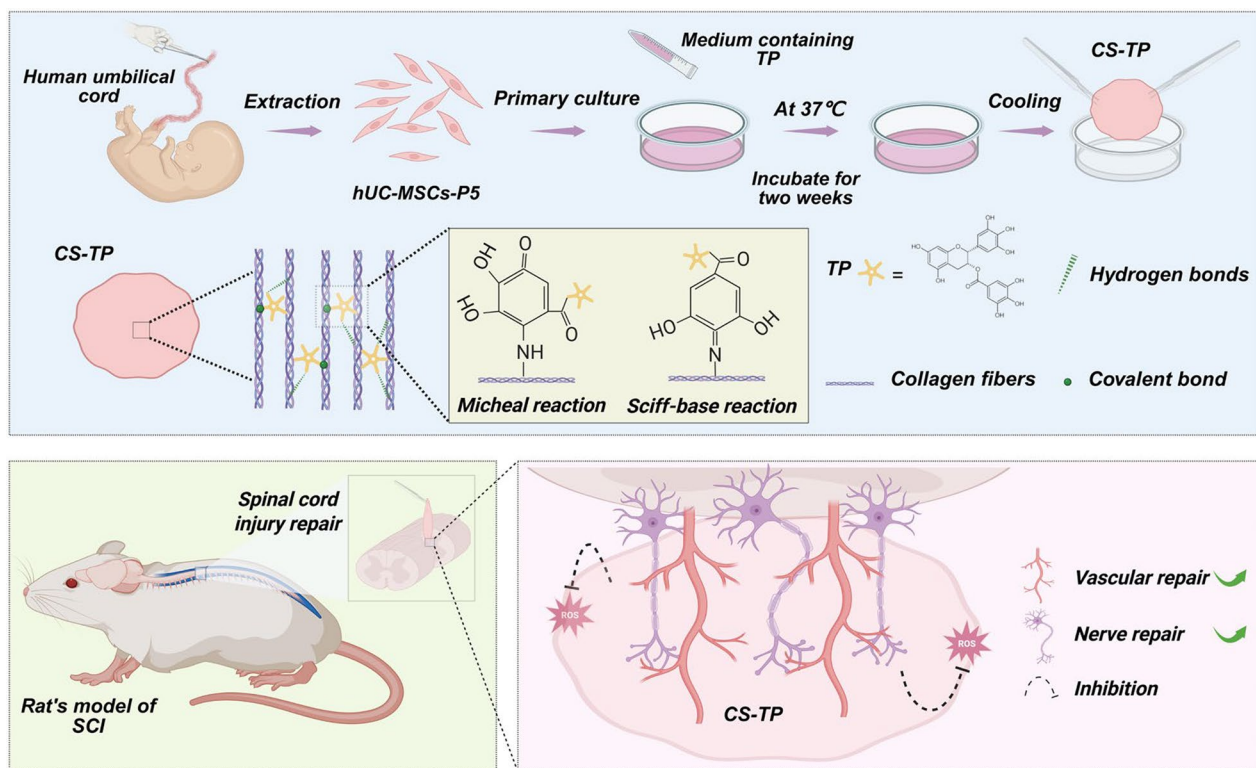


**Fig. 13** Schematic representation of the processes of creating the CS-TP and transplanting the CS-TP to the injury site in spinal cord injured rats. Created with BioRender.com

SCI recovery. This provides an approach for combining stem cell therapy with cell sheet technology to treat SCI.

#### Abbreviations

SCI	Spinal cord injury
ROS	Reactive oxygen species
hUC-MSCs	Human umbilical cord mesenchymal cells
ECM	Extracellular matrix
HUVECs	Human umbilical vein endothelial cells
EGCG	Epigallocatechin gallate
CS	Human umbilical cord mesenchymal stem cell sheet
ivc	Individually ventilated cage
SDS-PAGE	Sodium Dodecyl Sulfate Polyacrylamide Gel Electrophoresis
CS-TP	TP-loaded human umbilical cord mesenchymal stem cell sheet
MSCS	Mesenchymal stem cells
TP	Tea polyphenol
SD	Sprague-Dawley

#### Supplementary Information

The online version contains supplementary material available at <https://doi.org/10.1186/s13287-025-04376-5>.

Additional file 1.

#### Acknowledgements

The authors thank every collaborator on the team for their contributions and dedication. The author(s) disclosed receipt of the following financial support for the research, authorship, and/or publication of this article: National Natural Science Foundation of China (82371383); Grants from Jiangsu Provincial

Research Hospital (YJXY202204); Medical Research Projects of the Health Commission of Jiangsu Province (K2023006); Postgraduate Research & Practice Innovation Program of Jiangsu Province (SJCX24\_2061).

#### Author contributions

XQC designed the research and supervised the work. YLZ and CY performed the cell research. YLZ and HW performed animal research and drafted the manuscript. YLZ, CC, YL, CWY, TX, YCZ, ZCW, XRS, ZYZ and ZZY analyzed data and provided feedback. All the authors read and revised the final manuscript. The authors declare that they have not use AI-generated work in this manuscript.

#### Funding

This research was supported by the National Natural Science Foundation of China (82371383); Grants from Jiangsu Provincial Research Hospital (YJXY202204); Key Project of Jiangsu Provincial Health Committee (K2023006); Postgraduate Research & Practice Innovation Program of Jiangsu Province (SJCX24\_2061).

#### Availability of data and materials

The supporting materials can be obtained upon request via email to the corresponding authors.

#### Declarations

##### Ethics approval and consent to participate

The relevant procedures for extraction of human umbilical cord mesenchymal stem cells were approved by the Ethics Committee of Affiliated Hospital of Nantong University. The research project named "Mechanism of GelMA hydrogel encapsulation of umbilical cord mesenchymal stem cells spheroids promoting spinal cord injury repair" was approved on March 6, 2024 (No. 2024-L162) and informed consent was obtained from the donor



of each adipose tissue. The HUVECs and PC12 cell lines used in this study were purchased from Wuhan Procell Biotechnology Co., Ltd. The cells source company Procell obtained prior ethical approval to collect human cells, and all donors signed informed consent forms. All experimental procedures used in this study were approved by the Animal Care and Use Committee of Nantong University (Title of project: Mesenchymal Stem Cell Sheet Loaded with Plant Polyphenols Promote the Repair of Spinal Cord Injury; No. S20240720-004) and were following the National Research Council's Guide for the Care and Use of Laboratory Animals. Date of approval: 20/07/2024. The work has been reported in line with the ARRIVE guidelines 2.0.

#### Consent for publication

Not applicable.

#### Competing interests

The authors declare that they have no competing interests.

#### Author details

<sup>1</sup>Department of Spine Surgery, Affiliated Hospital of Nantong University, Nantong, China. <sup>2</sup>Medical School of Nantong University, Nantong, China.

Received: 5 November 2024 Accepted: 2 May 2025

Published online: 28 May 2025

#### References

- Fischer I, Dulin JN, Lane MA. Transplanting neural progenitor cells to restore connectivity after spinal cord injury. *Nat Rev Neurosci*. 2020;21(7):366–83.
- Nakamura M, Okano H. Cell transplantation therapies for spinal cord injury focusing on induced pluripotent stem cells. *Cell Res*. 2013;23(1):70–80.
- Doulames VM, Plant GW. Induced pluripotent stem cell therapies for cervical spinal cord injury. *Int J Mol Sci*. 2016;17(4):530.
- Pelaez-Vico MA, Fichman Y, Zandalinas SI, et al. ROS are universal cell-to-cell stress signals. *Curr Opin Plant Biol*. 2024;79: 102540.
- Yin Z, Wan B, Gong G, et al. ROS: executioner of regulating cell death in spinal cord injury. *Front Immunol*. 2024;15:1330678.
- Yan R, Zhang X, Xu W, Li J, Sun Y, Cui S, Xu R, Li W, Jiao L, Wang T. ROS-induced endothelial dysfunction in the pathogenesis of atherosclerosis. *Aging Dis*. 2024;16(1):250–68.
- Ji Y, Chen J, Pang L, et al. The acid sphingomyelinase inhibitor amitriptyline ameliorates TNF- $\alpha$ -induced endothelial dysfunction. *Cardiovasc Drugs Ther*. 2024;38(1):43–56.
- Hua R, Zhao C, Xu Z, et al. ROS-responsive nanoparticle delivery of ferroptosis inhibitor prodrug to facilitate mesenchymal stem cell-mediated spinal cord injury repair. *Bioact Mater*. 2024;38:438–54.
- Jin LY, Li J, Wang KF, et al. Blood-spinal cord barrier in spinal cord injury: a review. *J Neurotrauma*. 2021;38(9):1203–24.
- Jiang T, Qin T, Gao P, et al. SIRT1 attenuates blood-spinal cord barrier disruption after spinal cord injury by deacetylating p66Shc. *Redox Biol*. 2023;60: 102615.
- Li S, Dinh H, Matsuyama Y, et al. Molecular mechanisms in the vascular and nervous systems following traumatic spinal cord injury. *Life (Basel)*. 2022;13(1):9.
- Rajae A, Geisen ME, Sellers AK, et al. Repeat intravital imaging of the murine spinal cord reveals degenerative and reparative responses of spinal axons in real-time following a contusive SCI. *Exp Neurol*. 2020;327: 113258.
- Jiang L, Cao Y, Liu Z, et al. SRmuCT reveals 3D microstructural alterations of the vascular and neuronal network in a rat model of chronic compressive thoracic spinal cord injury. *Aging Dis*. 2020;11(3):603–17.
- Ford MC, Bertram JP, Hynes SR, et al. A macroporous hydrogel for the coculture of neural progenitor and endothelial cells to form functional vascular networks in vivo. *Proc Natl Acad Sci USA*. 2006;103(8):2512–7.
- Samanta S, Chakraborty S, Bagchi D. Pathogenesis of neurodegenerative diseases and the protective role of natural bioactive components. *J Am Nutr Assoc*. 2024;43(1):20–32.
- Takenaga M, Ohta Y, Tokura Y, et al. Lecithinized superoxide dismutase (PC-SOD) improved spinal cord injury-induced motor dysfunction through suppression of oxidative stress and enhancement of neurotrophic factor production. *J Control Release*. 2006;110(2):283–9.
- Xu L, Mu J, Ma Z, et al. Nanozyme-integrated thermoresponsive in situ forming hydrogel enhances mesenchymal stem cell viability and paracrine effect for efficient spinal cord repair. *ACS Appl Mater Interfaces*. 2023;15(31):37193–204.
- Liu X, Xu W, Zhang Z, et al. Vascular endothelial growth factor-transfected bone marrow mesenchymal stem cells improve the recovery of motor and sensory functions of rats with spinal cord injury. *Spine*. 2020;45(7):E364–72.
- Andrzejewska A, Dabrowska S, Lukomska B, et al. Mesenchymal stem cells for neurological disorders. *Adv Sci (Weinh)*. 2021;8(7):2002944.
- Shimizu K, Mitsuhashi T, Maeda Y, et al. Impact of intravenously administered cranial bone-derived mesenchymal stem cells on functional recovery in experimental spinal cord injury. *Neurosci Lett*. 2023;799: 137103.
- Gao Q, Zhao Y, Luo R, et al. Intrathecal umbilical cord mesenchymal stem cells injection alleviates neuroinflammation and oxidative stress in the cyclophosphamide-induced interstitial cystitis rats through the Sirt1/Nrf2/HO-1 pathway. *Life Sci*. 2023;331: 122045.
- Chen Y, Huang H, Li G, et al. Dental-derived mesenchymal stem cell sheets: a prospective tissue engineering for regenerative medicine. *Stem Cell Res Ther*. 2022;13(1):38.
- Chen J, Wang L, Liu M, et al. Implantation of adipose-derived mesenchymal stem cell sheets promotes axonal regeneration and restores bladder function after spinal cord injury. *Stem Cell Res Ther*. 2022;13(1):503.
- Okuda A, Horii-Hayashi N, Sasagawa T, et al. Bone marrow stromal cell sheets may promote axonal regeneration and functional recovery with suppression of glial scar formation after spinal cord transection injury in rats. *J Neurosurg Spine*. 2017;26(3):388–95.
- Zang Y, Zhang B, Zhang G, et al. Effects of combined treatment with hydrogen-rich electrolyzed water and tea polyphenols on oxidative stress, intestinal injury and intestinal flora disruption in heat-stressed mice. *J Therm Biol*. 2024;123: 103921.
- Huang Y, Wei Y, Xu J, et al. A comprehensive review on the prevention and regulation of Alzheimer's disease by tea and its active ingredients. *Crit Rev Food Sci Nutr*. 2023;63(30):10560–84.
- Ma L, Tan Y, Tong Q, et al. Collagen scaffolds functionalized by Cu(2+)-chelated EGCG nanoparticles with anti-inflammatory, anti-oxidation, vascularization, and anti-bacterial activities for accelerating wound healing. *Adv Healthc Mater*. 2024;13(12): e2303297.
- Zhao LL, Luo JJ, Cui J, et al. Tannic acid-modified decellularized tendon scaffold with antioxidant and anti-inflammatory activities for tendon regeneration. *ACS Appl Mater Interfaces*. 2024;16(13):15879–92.
- Sun L, Li B, Jiang D, et al. Nile tilapia skin collagen sponge modified with chemical cross-linkers as a biomedical hemostatic material. *Colloids Surf B Biointerfaces*. 2017;159:89–96.
- Ribeiro BF, Da CB, de Sousa BM, et al. Cell therapies for spinal cord injury: a review of the clinical trials and cell-type therapeutic potential. *Brain*. 2023;146(7):2672–93.
- Moratilla-Rivera I, Sanchez M, Valdes-Gonzalez JA, et al. Natural products as modulators of Nrf2 signaling pathway in neuroprotection. *Int J Mol Sci*. 2023;24(4):3748.
- Song D, Ge J, Wang Y, et al. Tea polyphenol attenuates oxidative stress-induced degeneration of intervertebral discs by regulating the Keap1/Nrf2/ARE pathway. *Oxid Med Cell Longev*. 2021;2021:6684147.
- Wang X, Ye L, Zhang K, et al. Upregulation of microRNA-200a in bone marrow mesenchymal stem cells enhances the repair of spinal cord injury in rats by reducing oxidative stress and regulating Keap1/Nrf2 pathway. *Artif Organs*. 2020;44(7):744–52.
- Du Yuchen-Zhang, MR, Zhang QY, et al. Armillariella tabescens-derived polysaccharides alleviated D-Gal-induced neuroinflammation and cognitive injury through enterocerebral axis and activation of keap-1/Nrf2 pathway. *Int J Biol Macromol*. 2024;273(Pt 1): 133035.
- Alam M, Ali S, Ashraf GM, et al. Epigallocatechin 3-gallate: from green tea to cancer therapeutics. *Food Chem*. 2022;379: 132135.
- Xu ZX, Zhang LQ, Zhou YN, et al. Histological and functional outcomes in a rat model of hemisection spinal cord with sustained VEGF/NT-3 release from tissue-engineered grafts. *Artif Cells Nanomed Biotechnol*. 2020;48(1):362–76.

37. Delfi I, Wood CR, Johnson L, et al. An in vitro comparison of the neurotrophic and angiogenic activity of human and canine adipose-derived mesenchymal stem cells (MSCs): translating MSC-based therapies for spinal cord injury. *Biomolecules*. 2020;10(9):1301.
38. Xie Y, Sun Y, Liu Y, et al. Targeted delivery of RGD-CD146(+)/CD271(+) human umbilical cord mesenchymal stem cell-derived exosomes promotes blood-spinal cord barrier repair after spinal cord injury. *ACS Nano*. 2023;17(18):18008–24.
39. Wang H, Zheng Z, Han W, et al. Metformin promotes axon regeneration after spinal cord injury through inhibiting oxidative stress and stabilizing microtubule. *Oxid Med Cell Longev*. 2020;2020:9741369.
40. Wang Y, Pei H, Chen W, et al. Palmatine protects PC12 cells and mice from Abeta25–35-induced oxidative stress and neuroinflammation via the Nrf2/HO-1 pathway. *Molecules*. 2023;28(24):7955.
41. Guo Q, Liu Q, Zhou S, et al. Apelin regulates mitochondrial dynamics by inhibiting Mst1-JNK-Drp1 signaling pathway to reduce neuronal apoptosis after spinal cord injury. *Neurochem Int*. 2024;180: 105885.
42. Takahashi A, Nakajima H, Kubota A, et al. Adipose-derived mesenchymal stromal cell transplantation for severe spinal cord injury: functional improvement supported by angiogenesis and neuroprotection. *Cells*. 2023;12(11):1470.
43. Zhang L, Li Y, Guan CY, et al. Therapeutic effect of human umbilical cord-derived mesenchymal stem cells on injured rat endometrium during its chronic phase. *Stem Cell Res Ther*. 2018;9(1):36.
44. Gao S, Jin Y, Ma J, et al. Preclinical study of human umbilical cord mesenchymal stem cell sheets for the recovery of ischemic heart tissue. *Stem Cell Res Ther*. 2022;13(1):252.
45. Guo R, Wan F, Morimatsu M, et al. Cell sheet formation enhances the therapeutic effects of human umbilical cord mesenchymal stem cells on myocardial infarction as a bioactive material. *Bioact Mater*. 2021;6(9):2999–3012.
46. Bou-Ghannam S, Kim K, Grainger DW, et al. 3D cell sheet structure augments mesenchymal stem cell cytokine production. *Sci Rep*. 2021;11(1):8170.
47. Yi Z, Cui X, Chen G, et al. Biocompatible, antioxidant nanoparticles prepared from natural renewable tea polyphenols and human hair keratins for cell protection and anti-inflammation. *ACS Biomater Sci Eng*. 2021;7(3):1046–57.
48. Li Q, Qiu Z, Wang Y, et al. Tea polyphenols alleviate hydrogen peroxide-induced oxidative stress damage through the Mst/Nrf2 axis and the Keap1/Nrf2/HO-1 pathway in murine RAW264.7 cells. *Exp Ther Med*. 2021;22(6):1473.
49. Abdelaala N, El-Shoura EAM, Khalaf MM, et al. Reno-protective impact of diosmin and perindopril in amikacin-induced nephrotoxicity rat model: modulation of SIRT1/p53/C-FOS, NF- $\kappa$ B-p65, and keap-1/Nrf2/HO-1 signaling pathways. *Immunopharmacol Immunotoxicol*. 2025;27:1–18.
50. Huang JY, Yuan YH, Yan JQ, et al. 20C, a bibenzyl compound isolated from *Gastrodia elata*, protects PC12 cells against rotenone-induced apoptosis via activation of the Nrf2/ARE/HO-1 signaling pathway. *Acta Pharmacol Sin*. 2016;37(6):731–40.
51. Wakabayashi N, Dinkova-Kostova AT, Holtzclaw WD, et al. Protection against electrophile and oxidant stress by induction of the phase 2 response: fate of cysteines of the Keap1 sensor modified by inducers. *Proc Natl Acad Sci USA*. 2004;101(7):2040–5.
52. Suttner DM, Dennery PA. Reversal of HO-1 related cytoprotection with increased expression is due to reactive iron. *FASEB J*. 1999;13(13):1800–9.
53. Huang L, Wang X, Zheng Y, et al. EGCG-NPs inhibition HO-1-mediated reprogram iron metabolism against ferroptosis after subarachnoid hemorrhage. *Redox Biol*. 2024;70: 103075.
54. Zhang B, Zeng M, Tie Q, et al. (-)-Epigallocatechin-3-gallate (EGCG) ameliorates ovalbumin-induced asthma by inhibiting inflammation via the TNF- $\alpha$ /TNF-R1/NLRP3 signaling pathway. *Int Immunopharmacol*. 2025;144: 113708.
55. He Z, Luo H, Wang Z, et al. Injectable and tissue adhesive EGCG-laden hyaluronic acid hydrogel depot for treating oxidative stress and inflammation. *Carbohydr Polym*. 2023;299: 120180.
56. Zhu W, Tang H, Cao L, et al. Epigallocatechin-3-O-gallate ameliorates oxidative stress-induced chondrocyte dysfunction and exerts chondroprotective effects via the Keap1/Nrf2/ARE signaling pathway. *Chem Biol Drug Des*. 2022;100(1):108–20.

## Publisher's Note

Springer Nature remains neutral with regard to jurisdictional claims in published maps and institutional affiliations.